ISSN 2523-6881

Volume 7, Issue 18 – January – June – 2023

Journal Renewable Energy

ECORFAN®

Journal Renewable Energy, Volume 7, Issue 18, January - June 2023, is a journal edited six monthly by ECORFAN-Peru. 1047 La Raza Avenue -Santa Ana, Cusco-Peru. WEB: www.ecorfan.org/taiwan, revista@ecorfan.org. Chief Editor: SERRANO-PACHECO, Martha. PhD. ISSN-On line: 2523-6881. Responsible for the latest update of this number ECORFAN Computer Unit. ESCAMILLA-BOUCHÁN, Imelda, PhD, LUNA-SOTO, Vladimir. PhD. 1047 La Raza Avenue -Santa Ana, Cusco-Peru, last updated June 30, 2023.

Journal Renewable Energy

Definition of Research Journal

Scientific Objectives

Support the international scientific community in its written production Science, Technology and Innovation in the Field of Engineering and Technology, in Subdisciplines Solar energy and its applications, renewable energies and climate change, environmental impact, hydroelectric plants, renewable energies, energy geothermal power in the world.

ECORFAN-Mexico SC is a Scientific and Technological Company in contribution to the Human Resource training focused on the continuity in the critical analysis of International Research and is attached to CONAHCYT-RENIECYT number 1702902, its commitment is to disseminate research and contributions of the International Scientific Community, academic institutions, agencies and entities of the public and private sectors and contribute to the linking of researchers who carry out scientific activities, technological developments and training of specialized human resources with governments, companies and social organizations.

Encourage the interlocution of the International Scientific Community with other Study Centers in Mexico and abroad and promote a wide incorporation of academics, specialists and researchers to the publication in Science Structures of Autonomous Universities - State Public Universities - Federal IES - Polytechnic Universities - Technological Universities - Federal Technological Institutes - Normal Schools - Decentralized Technological Institutes - Intercultural Universities - S & T Councils - CONAHCYT Research Centers.

Scope, Coverage and Audience

Journal Renewable Energy is a Research Journal edited by ECORFAN-Mexico S.C in its Holding with repository in Republic of Peru, is a scientific publication arbitrated and indexed with semester periods. It supports a wide range of contents that are evaluated by academic peers by the Double-Blind method, around subjects related to the theory and practice of Solar energy and its applications, renewable energies and climate change, environmental impact, hydroelectric plants, renewable energies, energy geothermal power in the world with diverse approaches and perspectives , That contribute to the diffusion of the development of Science Technology and Innovation that allow the arguments related to the decision making and influence in the formulation of international policies in the Field of Engineering and Technology. The editorial horizon of ECORFAN-Mexico® extends beyond the academy and integrates other segments of research and analysis outside the scope, as long as they meet the requirements of rigorous argumentative and scientific, as well as addressing issues of general and current interest of the International Scientific Society.

Editorial Board

Arbitration Committee

Assignment of Rights

The sending of an Article to Journal Renewable Energy emanates the commitment of the author not to submit it simultaneously to the consideration of other series publications for it must complement the Originality Format for its Article.

The authors sign the Authorization Format for their Article to be disseminated by means that ECORFAN-Mexico, S.C. In its Holding Republic of Peru considers pertinent for disclosure and diffusion of its Article its Rights of Work.

Declaration of Authorship

Indicate the Name of Author and Coauthors at most in the participation of the Article and indicate in extensive the Institutional Affiliation indicating the Department.

Identify the Name of Author and Coauthors at most with the CVU Scholarship Number-PNPC or SNI-CONAHCYT- Indicating the Researcher Level and their Google Scholar Profile to verify their Citation Level and H index.

Identify the Name of Author and Coauthors at most in the Science and Technology Profiles widely accepted by the International Scientific Community ORC ID - Researcher ID Thomson - arXiv Author ID - PubMed Author ID - Open ID respectively.

Indicate the contact for correspondence to the Author (Mail and Telephone) and indicate the Researcher who contributes as the first Author of the Article.

Plagiarism Detection

All Articles will be tested by plagiarism software PLAGSCAN if a plagiarism level is detected Positive will not be sent to arbitration and will be rescinded of the reception of the Article notifying the Authors responsible, claiming that academic plagiarism is criminalized in the Penal Code.

Arbitration Process

All Articles will be evaluated by academic peers by the Double Blind method, the Arbitration Approval is a requirement for the Editorial Board to make a final decision that will be final in all cases. MARVID® is a derivative brand of ECORFAN® specialized in providing the expert evaluators all of them with Doctorate degree and distinction of International Researchers in the respective Councils of Science and Technology the counterpart of CONAHCYT for the chapters of America-Europe-Asia- Africa and Oceania. The identification of the authorship should only appear on a first removable page, in order to ensure that the Arbitration process is anonymous and covers the following stages: Identification of the Research Journal with its author occupation rate - Identification of Authors and Coauthors - Detection of plagiarism PLAGSCAN - Review of Formats of Authorization and Originality-Allocation to the Editorial Board- Allocation of the pair of Expert Arbitrators-Notification of Arbitration -Declaration of observations to the Author-Verification of Article Modified for Editing-Publication.

Instructions for Scientific, Technological and Innovation Publication

Knowledge Area

The works must be unpublished and refer to topics of Solar energy and its applications, renewable energies and climate change, environmental impact, hydroelectric plants, renewable energies, energy geothermal power in the world and other topics related to Engineering and Technology.

Presentation of the content

In the first article we present, *Design of a p-i-n type inverted perovskite solar cell using SiO_x as down-conversion material to improve PCE: Simulation and optimization in SCAPS-1D* by PAZ-TOTOLHUA, Ezequiel, CARRILLO-LÓPEZ, Jesús, LUNA-LÓPEZ, José Alberto and BENÍTEZ-LARA, Alfredo, with adscription in the Benemérita Universidad Autónoma de Puebla, in the next article we present *Low-cost Schlieren system for flow visualization in transparent media in the wind sector* by URIBE-CASTILLO, Citlali & RICO-ESPINO, José Guadalupe, with adscription in the Universidad Tecnológica de Querétaro, in the next article we present, *Effect of dye on the efficiency of Grätzel cells* by BERNAL-MARTINEZ, Guillermo, MONTES-GUTIERREZ, Jorge, GARCIA-GUTIERREZ, Rafael and CONTRERAS-LOPEZ, Oscar, with adscription in the Centro de Investigación Científica y de Educación Superior de Ensenada, Universidad Nacional Autónoma de México and Universidad de Sonora, in the last article we present, *Economic and environmental dispatch of power systems: Minimising CO_2 emissions* by integrating renewable energy sources by GARCÍA-GUZMÁN, José Miguel, RAZÓN-GONZÁLEZ, Juan Pablo, CANO-LARA, Miroslava and GONZÁLEZ-PONCE, María del Refugio, with adscription in the Instituto Tecnológico Superior de Irapuato and Universidad Incarnate Word Campus Bajío.

Content

Article	Page
Design of a p-i-n type inverted perovskite solar cell using SiO_x as down-conversion material to improve PCE: Simulation and optimization in SCAPS-1D PAZ-TOTOLHUA, Ezequiel, CARRILLO-LÓPEZ, Jesús, LUNA-LÓPEZ, José Alberto and BENÍTEZ-LARA, Alfredo *Benemérita Universidad Autónoma de Puebla*	1-8
Low-cost Schlieren system for flow visualization in transparent media in the wind sector URIBE-CASTILLO, Citlali & RICO-ESPINO, José Guadalupe *Universidad Tecnológica de Querétaro*	9-18
Effect of dye on the efficiency of Grätzel cells BERNAL-MARTINEZ, Guillermo, MONTES-GUTIERREZ, Jorge, GARCIA-GUTIERREZ, Rafael and CONTRERAS-LOPEZ, Oscar *Centro de Investigación Científica y de Educación Superior de Ensenada* *Universidad Nacional Autónoma de México* *Universidad de Sonora*	19-24
Economic and environmental dispatch of power systems: Minimising CO_2 emissions by integrating renewable energy sources GARCÍA-GUZMÁN, José Miguel, RAZÓN-GONZÁLEZ, Juan Pablo, CANO-LARA, Miroslava and GONZÁLEZ-PONCE, María del Refugio *Instituto Tecnológico Superior de Irapuato* *Universidad Incarnate Word Campus Bajío*	25-31

Article **Journal Renewable Energy**
June, 2023 Vol.7 No.18 1-8

Design of a p-i-n type inverted perovskite solar cell using SiO_x as down-conversion material to improve PCE: Simulation and optimization in SCAPS-1D

Diseño de una celda solar de perovskita tipo p-i-n utilizando SiO_x como material de energía de conversión descendente para mejorar el PCE: Simulación y optimización en SCAPS-1D

PAZ-TOTOLHUA, Ezequiel[1]†*, CARRILLO-LÓPEZ, Jesús[1], LUNA-LÓPEZ, José Alberto[1] and BENÍTEZ-LARA, Alfredo[2]

[1]*Benemérita Universidad Autónoma de Puebla, Centro de Investigaciones en Dispositivos Semiconductores (CIDS-ICUAP), Av. San Claudio y 14 sur, Edificios IC5 y IC6, C. U., Col. San Manuel, Puebla, Pue. 72570, México.*
[2]*Centro de Investigaciones en Óptica A.C., Lomas del Bosque 115, León, Guanajuato. 37150, México.*

ID 1st Autor: *Ezequiel, Paz-Totolhua* / **ORC ID:** 0000-0001-6826-5353, **CVU CONAHCYT ID**: 712701

ID 1st Co-author: *Jesús, Carrillo-López* / **ORC ID:** 0009-0002-9036-6999, **CVU CONAHCYT ID**: 5242

ID 2nd Co-author: *Jose Alberto, Luna-López* / **ORC ID:** 0000-0002-7647-3184, **CVU CONAHCYT ID**: 200808

ID 3rd Co-author: *Alfredo, Benítez-Lara* / **ORC ID:** 0000-0002-7206-2767, **CVU CONAHCYT ID**: 256851

DOI: 10.35429/JRE.2023.18.7.1.8 Received March 16, 2023; Accepted June 30, 2023

Abstract

In this research work, an inverted p-i-n type perovskite solar cell: ITO/PEDOT: PSS/$CH_3NH_3PbI_3$/PCBM/Au has been simulated and optimized in SCAPS-1D. The optimized parameters in SCAPS-1D that improved solar performance were: perovskite thickness, the total defect density of perovskite, the total defect density of interfaces, series and shunt resistances, and device operating temperature. As a result, the efficiency (PCE) increased to 18.33%. Subsequently, when the silicon-rich oxide (SiOx) material was implemented in the simulation as down-conversion energy material on the outside of the cell, a power conversion efficiency (PCE) of 23.7% was obtained. The SiO_X film obtained experimentally by sputtering obtained good photoluminescence, absorption coefficient, band gap, and transmittance characteristics before and after thermal annealing. These characteristics have been considered for the proposed device. It is indicated that the inverted perovskite solar cell of type p-i-n: SiO_x/ITO/PEDOT:PSS/$CH_3NH_3PbI_3$/PCBM/Au has better J-V output values and EQ quantum efficiency than the perovskite solar cell without SiOx.

Perovskite, Efficiency, Simulated

Resumen

En este trabajo de investigación, una celda solar de perovskita tipo p-i-n invertida: ITO/PEDOT: PSS/$CH_3NH_3PbI_3$/PCBM/Au ha sido simulada y optimizada en el software SCAPS-1D. Los parámetros optimizados en SCAPS-1D que mejoraron el rendimiento solar fueron: el grosor de la perovskita, la densidad total de defectos de la perovskita, la densidad total de defectos de las interfaces, las resistencias en serie y derivación y la temperatura de operación del dispositivo. Como resultado de esto, la eficiencia (PCE) incrementó a 18.33%. Posteriormente, cuando se implementó en la simulación el óxido rico en silicio (SiOx) como material de energía de conversión descendente en la parte externa de la celda, se obtuvo una eficiencia (PCE) de 23.7 %. La película de SiO_X obtenida experimentalmente por sputtering obtuvo buenas características de fotoluminiscencia, coeficiente de absorción, band gap y transmitancia antes y después del recocido térmico. Estas características fueron consideraras en el dispositivo propuesto. Se concluye que la celda solar de perovskita: SiO_x/ITO/PEDOT: PSS/$CH_3NH_3PbI_3$/PCBM/Au tiene mejores valores de salida J-V y eficiencia cuántica EQ que la celda solar sin SiO_x.

Perovskita, Eficiencia, Simulado

Citation: PAZ-TOTOLHUA, Ezequiel, CARRILLO-LÓPEZ, Jesús1, LUNA-LÓPEZ, José Alberto and BENÍTEZ-LARA, Alfredo. Design of a p-i-n type inverted perovskite solar cell using SiOx as down-conversion material to improve PCE: Simulation and optimization in SCAPS-1D. Journal Renewable Energy. 2023. 7-18: 1-8

*Correspondence to Author (e-mail: ezequiel.paz@alumno.buap.mx)
† Researcher contributing as first author.

Introduction

Perovskite solar cells (PSCs) have become a principal source of research since their emergence in 2009. They are currently the most promising devices of the future for use as a renewable energy source. In just a few years, they have made remarkable progress as their efficiency has been certified up to 25.5 %, comparable to silicon (Si), gallium arsenide (GaAs), and cadmium telluride (CdTe) technology, according to Chao *et al*., (2021). Until now, most perovskite solar cells (PSCs) have been fabricated with the traditional vertical or n-i-p type structure. Notwithstanding, these devices suffer from severe hysteresis effects and have poor stability. In contrast, the inverted or p-i-n type cell has good, fewer defective states between interfaces it is possible to fabricate devices at low temperatures (Yang *et a*l., 2022).

Notwithstanding, metal-organic perovskite ($CH_3NH_3PbI_3$) remains one of the materials used in perovskite solar cells due to its simple synthesis process, low cost, and high performance (Yin *et al*., 2022). Nevertheless, its instability and easy degradation due to environmental factors are still an obstacle to its commercialization (Mazumdar *et al*., 2021). Perovskite $CH_3NH_3PbI_3$ has many advantages as a high absorption coefficient, tunable band gap, high charge carrier mobility, low trap density, long carrier diffusion length, and small exciton binding energy (Mohanty *et al*., 2019).

Researchers are exploring a lot in the field of perovskites as the use of different structures in solar cells, the design of new hole and electron transport materials, the improvement of perovskite materials, and the implementation of interlayers to achieve higher efficiency and improved spectral response. Improving the utilization of the incident solar spectrum may be one of the approaches to increase the performance of these devices because currently, perovskite solar cells can only utilize a fraction of the incident solar photons, ranging from the visible to the near infrared (Datt, Bishnoi, Lee, *et al*., 2022). That is ultraviolet (UV) regions are not used and are considered harmful.

According to the literature, a down-conversion energy material absorbs the short wavelength photons of the solar spectrum, which the solar cell does not use efficiently, and re-emits them at longer wavelengths (Hosseini & Ghanbari, 2018). The main characteristics of a down-conversion energy material are high photoluminescence quantum efficiency (PLQE), photochemical and environmental stability, broadband absorption in the region where the spectral response of the solar cell is low, high absorption coefficient in low wavelength region, high transmittance and broadband emission, particularly in the region where the device response is high, sufficient stokes shift to minimize the self-absorption energy losses due to the spectral overlap between the absorption and emission bands, low cost, easy to process and can be deposited by the large scalable method, and low film roughness (Datt, Bishnoi, Hughes, *et al*., 2022).

An alternative to solve spectral mismatch losses, improve stability, and increase efficiency is to apply a silicon-rich oxide (SiO_x) layer on the surface of a perovskite solar cell. This material is a silicon oxide out of stichometry that contains small silicon islands embedded in a silicon dioxide matrix and stands out for its high photoluminescence intensity of red light when illuminated with ultraviolet UV radiation (Vivaldo *et al*., 2016).

In this work, the photovoltaic characteristics of a SiOx film deposited by co-sputtering have been reviewed for implementation in perovskite solar cells. Subsequently, an inverted perovskite solar cell type p-i-n: ITO/PEDOT: PSS/$CH_3NH_3PbI_3$/PCBM/Au was numerically simulated. Photovoltaic parameters such as perovskite thickness, total defect densities, series and shunt resistances, and operating temperature were optimized for this device, reaching an efficiency of 18.33 %. The J-V output values were compared with those reported experimentally. Finally, a new device model was proposed: SiO_x/ITO/PEDOT: PSS/$CH_3NH_3PbI_3$/PCBM/Au, which includes a down-conversion energy material (SiO_x) on the outside, and whose efficiency increased to 23.74 %. In the latter simulation, the J-V output characteristics and QE quantum efficiency were better than those of the device without SiO_x.

ISSN 2523-2881

PAZ-TOTOLHUA, Ezequiel, CARRILLO-LÓPEZ, Jesús1, LUNA-LÓPEZ, José Alberto and BENÍTEZ-LARA, Alfredo. Design of a p-i-n type inverted perovskite solar cell using SiOx as down-conversion material to improve PCE: Simulation and optimization in SCAPS-1D. Journal Renewable Energy. 2023

Numerical methodology

Solar cell structure

The simulated inverted perovskite solar cell has the configuration ITO/PEDOT: PSS/$CH_3NH_3PbI_3$/PCBM/Au, where indium doped tin oxide (ITO) is the front contact; poly (3,4- ethylenedioxythiophene) polystyrene sulfonate (PEDOT: PSS) is the hole transport layer; $CH_3NH_3PbI_3$ is the absorber layer; Phenyl-C61-butyric acid and methyl ester (PCBM) is the electron transport layer; and gold (Au) is the back metal contact. In addition to the proposed model SiO_x/ITO/PEDOT/$CH_3NH_3PbI_3$/PCBM/Au is a device that includes an outer layer of silicon-rich oxide (SiO_x), which works as a down-conversion energy material. The two solar structures are represented in Figure 1 (a, b) and the energy band diagram is shown in Figure 1 (c).

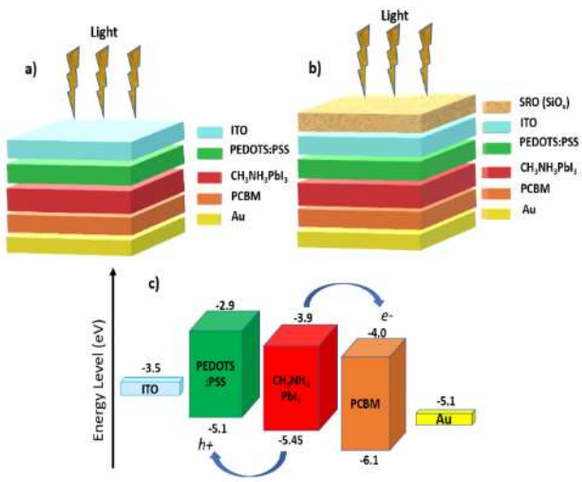

Figure 1 (a) Schematic diagram of perovskite solar cell; (b) Schematic diagram of perovskite solar cell with SiO_x; (c) Energy band gap diagram
Source: Own elaboration, Paint 3D

Numerical method

The simulation was performed in SCAPS-1D software version 3.3.10 under AM1.5G illumination at 300 K ambient temperature. The SCAPS-1D software, developed at the Department of Electronics and Information Systems (ELIS) at the University of Ghent in Belgium, has been used to model and simulate solar cells (Burgelman *et al*., 2000). The software solves the semiconductor equations in one dimension in a steady state (Decock *et al*., 2013) and (Burgelman *et al*., 2013).

The main equations it solves are the Poisson equation (1), the electron continuity equation (2), the hole continuity equation (3), the electron charge transport equation (4), the hole charge transport equation (5), and the absorption coefficient (6), which are solved until convergence occurs (Verschraegen & Burgelman, 2007).

Poisson equation:

$$\frac{dE}{dx} = \frac{q}{\varepsilon_0 \varepsilon_r}[p(x) - n(x) + N_D^+(x) - N_A^-(x) + p_t(x) - n_t(x)] \quad (1)$$

Where E is the electric field, q is electronic charge, ε_0 is permittivity of vacuume, ε_r is relative permittivity, N_D^+ is the shallow donor impurity density, $N_A^+$is the shallow aceptor impurity density, $n(x)$ and $p(x)$ are the densities of electrons and holes. Similarly $p_t(x)\ y\ n_t(x)$represent the trapped holes and electrons as a function of x respectively.

Continuity equations:

$$\frac{dJ_n}{dx} = G - U_n \quad (2)$$

$$\frac{dJ_p}{dx} = G - U_p \quad (3)$$

Where J_n and J_p are the electron and hole current densities, G is the generation rate, U_n and U_p are the recombination rates for electrons and holes respectively.

Charge transport equation:

$$J_n = D_n \frac{dn}{dx} + \mu_n n \frac{d\phi}{dx} \quad (4)$$

$$J_p = D_p \frac{dp}{dx} + \mu_p p \frac{d\phi}{dx} \quad (5)$$

Where $D_n$and $D_p$are the electron and hole diffusion coefficients respectively, μ_n and μ_p are the electron and hole mobility respectively.

Absorption coefficient equation:

$$\alpha(\lambda) = (A + \frac{B}{h\nu})\sqrt{h\nu - E_g} \quad (6)$$

Where $A$and B are constants, h is Planck constant, ν is frequency of photon and E_g is the band gap of the absorber layer.

ISSN 2523-2881

Simulation parameters

The physical, optical, and electrical parameters were obtained from the scientific literature and summarized in Table 1 (Basyoni *et al*., 2021; A. Ghosh *et a*l., 2020; B. Ghosh *et al*., 2022; Jamal *et a*l., 2019; Sabbah *et al*., 2022). The parameters used for the silicon-rich oxide SiO_x correspond to a SiO_2 film. Nevertheless, the absorption coefficient, the photoluminescence, and the band gap are the results of the characterization of the deposits obtained by co-sputtering for this work. In addition, the work function for the metal contact (Au) was 5.1 eV.

Photovoltaic Parameters	SiOx	ITO	PEDOTS: PSS	$CH_3HN_3PbI_3$	PCBM
Thickness (nm)	90	100	40	300	80
Energy Band gap, *Eg* (eV)	4.5	3.5	2.2	1.57	2.1
Electron affinity, χ (eV)	0.950	2.3	2.9	3.9	4.1
Dielectric permittivity, *εr*	3.9	9	2.3	18	4
Effective Density of stated at conduction band, *Nc* ($1/cm^3$)	2.8×10^{18}	2.2×10^{18}	2.2×10^{18}	2.2×10^{18}	2.5×10^{19}
Effective Density of stated at valence band, *Nv* ($1/cm^3$)	2.6×10^{19}	1.8×10^{19}	2.8×10^{18}	1.9×10^{19}	2.5×10^{19}
Electron thermal velocity, Vh (cm/s)	1×10^7	1×10^7	1×10^7	1×10^7	1×10^7
Hole thermal velocity, Ve (cm/s)	1×10^7	1×10^7	1×10^7	1×10^7	1×10^7
Hole mobility, *μn* (cm^2/Vs)	1.5×10^3	31	0.0002	3	0.01
Electron Mobility, *μp* (cm^2/Vs)	4.5×10^3	50	0.02	17	0.01
Uniform Shallow Donor Dopping, N_D ($1/cm^3$)	0	0	0	0	5×10^{17}
Uniform Shallow Acceptor Dopping, N_A ($1/cm^3$)	2.0×10^{18}	2.0×10^{16}	1×10^{18}	0	0
Defect density, *Nt* ($1/cm^3$)	10^{15}	10^{15}	10^{15}	10^{15}	10^{15}

Table 1 Optical and electrical parameters for simulation
Source: Own elaboration, summary of bibliography

Figure 2 shows the definition and editing panel in the SCAPS-1D software. In this section, you can enter and edit the electrical and optical parameters of the layers, the direction of light incidence, and the interface parameters.

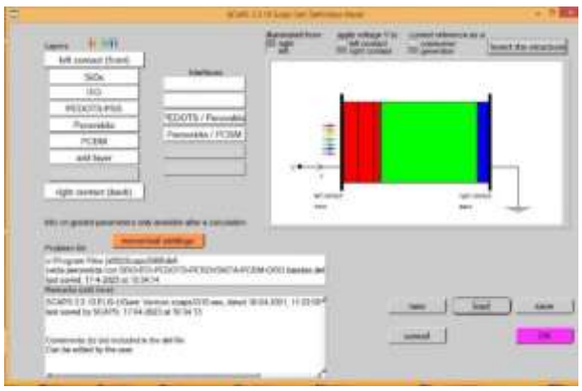

Figure 2 Definition and editing panel in the SCAPS-1D simulator
Source: SCAPS-1D Software version 3.3.10

Results and discusión

Photoluminescence, absorption coefficient, band gap, and transmittance of SiO_x

The silicon-rich oxide (SiO_x) film was deposited by co-sputtering on 1" x 1" x 1 mm quartz substrates, obtaining a thickness of 90 nm with low roughness. The SiO_x film was deposited by simultaneous sputtering of Si and SiO_2 targets. The equipment used for the deposition was a magnetron sputtering system. The deposition parameters were estimated to reach an average silicon excess (5.9 at. %) to achieve a maximum photoluminescence emission in the red region, according to Coyopol *et al*., (2018).

Graph 1 shows the PL photoluminescence spectrum, where it is observed that SiO_x has PL emission in the red-blue region before and after thermal annealing. SiO_x before annealing shows a dominant emission peak at 423 nm, with two smaller peaks at 640 nm and 780 nm after deconvolution. After thermal annealing at 1100°C for 2 hours, the film obtained two emission peaks, one in the red region (775 nm) and another of lower intensity in the blue region (418 nm). The PL emission peaks are associated with the complete activation of Si=O defects, favored by the average size of silicon nanocrystals embedded in a silicon-rich oxide dielectric matrix (Coyopol *et al*., 2016).

ISSN 2523-2881

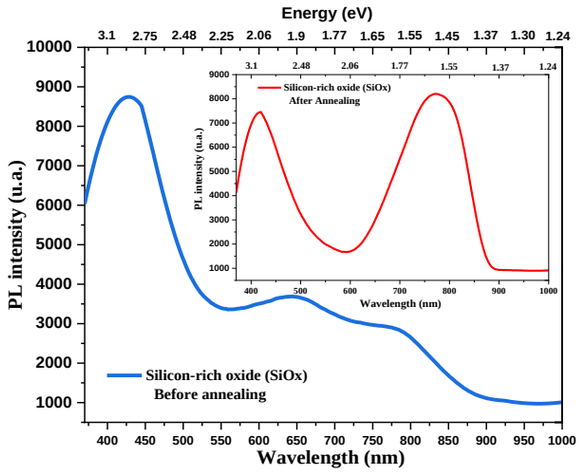

Graph 1 Photoluminescence spectra of silicon-rich oxide (SiO_x) before and after thermal annealing
Source: Own elaboration, OriginPro 2018

Graph 2 shows the absorption coefficient and band gap obtained from the SiO_x film after thermal annealing. The graph shows that the film has a high absorption coefficient in the low wavelength region (ultraviolet UV). In addition, the film has a low absorption coefficient in the range from 350 nm to 800 nm, which corresponds to the visible spectrum.The band gap energy was estimated using the Tauc relation and the Beer Lambert equation. This absorption coefficient and the band gap have been used in the SCAPS-1D simulator.

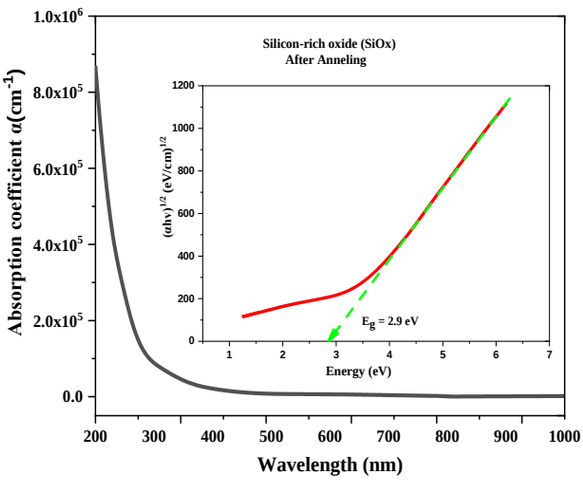

Graph 2 Absorption coefficient of silicon-rich oxide (SiOx)
Source: Own elaboration, OriginPro 2018

Graph 3 shows the transmittance spectrum of the SiO_x film after thermal annealing. The graph shows that the film has a transmittance above 90% in the range from 400 nm to 800 nm, which is the visible spectrum.

In addition, the film shows a progressive decrease in transmittance in the 200 nm to 400 nm range, which corresponds to the ultraviolet spectrum. These results agree with the absorption coefficient, concluding that the spectral response of the SiO_x film is concentrated in the ultraviolet region.

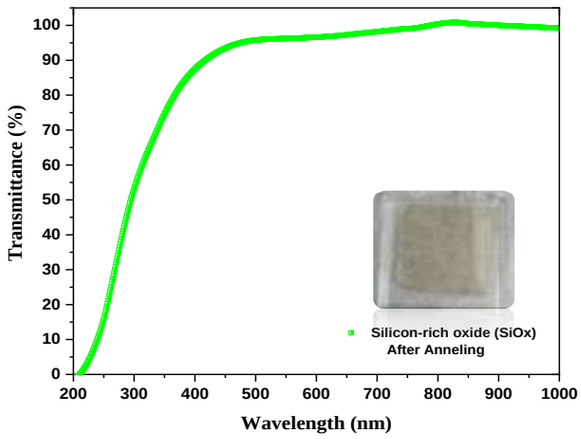

Graph 3 Transmittance spectrum of silicon-rich oxide (SiO_x)
Source: Own elaboration, OriginPro 2018

J-V current-voltage curve, EQ quantum efficiency, and band diagram

This section shows the J-V plot, QE quantum efficiency plot, and energy band diagram of the perovskite solar cell: ITO/PEDOT:PSS/$CH_3NH_3PbI_3$/PCBM/Au and the proposed perovskite solar cell: SiO_x/ITO/PEDOT:PSS/$CH_3NH_3PbI_3$/PCBM/Au. Furthermore, we have considered the optimum values obtained from the SCAPS-1D simulation. Table 2 shows the optimal values for perovskite thickness, total defect density, series and shunt resistance, and solar cell operating temperature. The parameters were varied in the simulator, keeping the other parameters constant.

Parameters	Variation range	Optimal value
Perovskite thickness	50-1000 nm	500 nm
Perovskite defect density	10^{10}-10^{20} cm^{-3}	10^{13} cm^{-3}
Defect density of PEDOTS:PSS/Perovskite interface	10^{10}-10^{20} cm^{-3}	10^{13} cm^{-3}
Defect density of Perovskite/PCBM interface	10^{10}-10^{20} cm^{-3}	10^{13} cm^{-3}
Series Resistance	10-100 $\Omega.cm^2$	10 $\Omega.cm^2$
Shunt Resistance	500-5000 $\Omega.cm^2$	5000 $\Omega.cm^2$
Operating temperature of the solar cell	300-390 K	300 K

Table 2 Optimal values obtained from SCAPS-1D
Source: Own Elaboration

ISSN 2523-2881

Simulation of the perovskite solar cell: ITO/PEDOT: PSS/$CH_3NH_3PbI_3$/PCBM/Au produced output values of Voc = 1.112 V, Jsc =20.236 mA/cm^2, FF = 81.24 % and PCE =18.33 %, similar to those reported experimentally, according to Heo *et al*., (2015).

Notwithstanding, the proposed perovskite solar cell:SiO_x /ITO/PEDOT:PSS/$CH_3NH_3PbI_3$/PCBM/Au, containing a SiO_x monolayer film, produced output values of Voc = 1.088 V, Jsc =27.236 mA/cm^2, FF = 80.06 % and PCE = 23.74 %. Graph 4 shows the J-V curves with the output values of both devices.

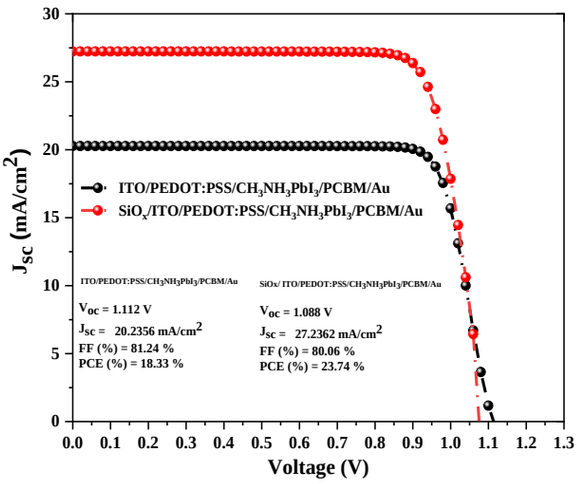

Graph 4 J-V curve of perovskite solar cell with and without SiO_x
Source: Own Elaboration, OriginPro 2018

Graph 5 shows the QE quantum efficiency for both devices. An improvement in the QE quantum efficiency is observed for the solar cell that includes the SiO_x film compared to the one that does not. The range of enhancement is observed mainly in the wavelength range from 500 to 780 nm. This increase determines that the structure with the SiO_x film has a better spectral response.

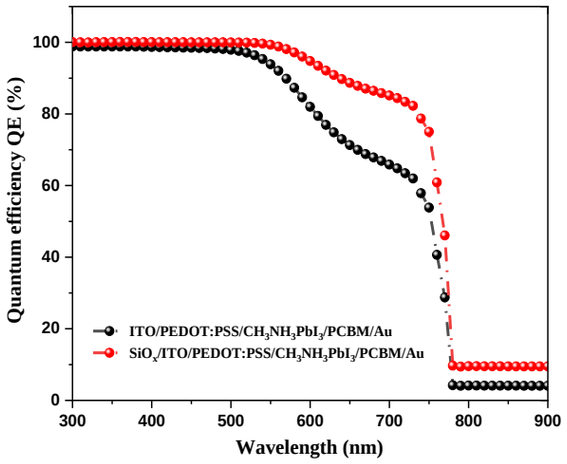

Graph 5 QE Quantum efficiency of perovskite solar cell with and without SiO_x
Source: Own Elaboration, OriginPro 2018

Graph 6 shows the band diagram of the perovskite solar cell with the optimized parameters and the SiO_x down-conversion material. It is observed that there is a splitting of the valence band and conduction band. In addition, the energy band diagram indicates that both the PEDOTS: PSS material and the PCBM material have higher energy bandwidths compared to the absorber layer ($CH_3NH_3PbI_3$), so there is a band alignment, favoring the passage of electrons and holes generated in the perovskite. Meanwhile, the energy barriers at the interfaces ensure the diffusion of carriers generated in the perovskite into the hole and electron transport layers. Finally, the transparent SiO_x material filters visible light due to its wide band gap and, at the same time, absorbs ultraviolet light, which contributes to increasing the photocurrent.

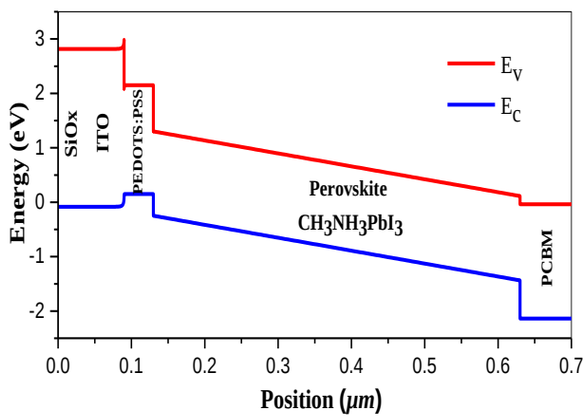

Graph 6 Energy band diagram of perovskite solar cell with SiO_x
Source: Own Elaboration, OriginPro 2018 and SCAPS-1D

ISSN 2523-2881

Acknowledgments

The authors thank the laboratories of INAOE, CIMAV, CIO, and CIDS-BUAP for their help in obtaining and characterizing the samples.

Funding

This work has been funded by CONAHCYT [grant number: 712701].

Conclusions

A p-i-n type inverted perovskite solar cell: ITO/PEDOT:PSS/$CH_3NH_3PbI_3$/PCBM/Au has been simulated and optimized in SCAPS-1D software.

The optimal values obtained from the simulation indicate that a perovskite layer thickness of 500 nm, a total defect density at the perovskite and interfaces of 10^{13} cm^{-3}, a series and shunt resistance of 10 $\Omega.cm^2$ and 5000 $\Omega.cm^2$ respectively, and an operating temperature of 300 K improve the performance of the solar cell.

In addition, the experimentally obtained silicon-rich oxide (SiOx) material has the main characteristics of an energy down-conversion material for application in perovskite solar cells. In conclusion, the solar device: SiOx/ITO/PEDOT:PSS/$CH_3NH_3PbI_3$/PCBM/Au has the potential to generate a higher photocurrent, as the simulation results in an improved efficiency of 23.74 %, while the solar device without the SiOx film: ITO/ PEDOT:PSS/$CH_3NH_3PbI_3$/PCBM/Au produces an efficiency of 18.33 %, slightly higher than the experimental data, i.e. 18.1 %. The perovskite solar cell with SiOx is considered efficient, as it has a simple architecture in addition to the fact that it can easily obtain experimental verification.

References

Basyoni, M. S. S., Salah, M. M., Mousa, M., Shaker, A., Zekry, A., Abouelatta, M., Alshammari, M. T., Al-Dhlan, K. A., & Gontrand, C. (2021). On the Investigation of Interface Defects of Solar Cells: Lead-Based vs Lead-Free Perovskite. *IEEE Access*, *9*, 130221–130232. https://doi.org/10.1109/ACCESS.2021.3114383

Burgelman, M., Decock, K., Kheli, S., & Abass, A. (2013). Advanced electrical simulation of thin film solar cells. *Thin Solid Films*, *535*, 296–301. https://doi.org/doi:10.1016/j.tsf.2012.10.032

Burgelman, M., Nollet, P., & Degrave, S. (2000). Modelling polycrystalline semiconductor solar cells. *Thin Solid Films*, *361*, 527–532. https://doi.org/doi:10.1016/s0040-6090(99)00825-1

Chao, L., Niu, T., Gao, W., Ran, C., Song, L., Chen, Y., & Huang, W. (2021). Solvent Engineering of the Precursor Solution toward Large-Area Production of Perovskite Solar Cells. *Advanced Materials*, *33*(14), 1–23. https://doi.org/10.1002/adma.202005410

Coyopol, A., Cardona, M. A., Díaz Becerril, T., Licea Jimenez, L., & Morales Sánchez, A. (2016). Silicon excess and thermal annealing effects on structural and optical properties of co-sputtered SRO films. *Journal of Luminescence*, *176*, 40–46. https://doi.org/10.1016/j.jlumin.2016.02.033

Coyopol, A., Díaz, T., Garcia, G., Cabañas, S., Palacios, L., & Morales, A. (2018). Synthesis and Luminescent Properties of Silicon Nanocrystals. *IntechOpen*, *11*(tourism), 13. https://doi.org/http://dx.doi.org/10.5772/intechopen.74286

Datt, R., Bishnoi, S., Hughes, D., Mahajan, P., Singh, A., Gupta, R., Arya, S., Gupta, V., & Tsoi, W. C. (2022). Downconversion Materials for Perovskite Solar Cells. *Solar RRL*, *2200266*, 2200266. https://doi.org/10.1002/solr.202200266

Datt, R., Bishnoi, S., Lee, H. K. H., Arya, S., Gupta, S., Gupta, V., & Tsoi, W. C. (2022). Down- conversion materials for organic solar cells: Progress, challenges, and perspectives. *Aggregate*, *3*(3), 1–21. https://doi.org/10.1002/agt2.185

Decock, K., Khelifi, S., & Burgelman, M. (2013). Modelling and measurement of the metastable defect distribution in chalcopyrite-based thin film solar cells. *Thin Solid Films*, *535*(1), 362–365. https://doi.org/10.1016/j.tsf.2012.10.078

Ghosh, A., Dipta, S., Nikor, S., Saqib, N., & Saha, A. (2020). Performance analysis of an efficient and stable perovskite solar cell and a comparative study of incorporating metal oxide transport layers. *Journal of the Optical Society of America B*, *37*(7), 1966. https://doi.org/10.1364/josab.391817

Ghosh, B., Nasir, S., Chee, F., Routray, S., Saad, I., & Mohamad, K. (2022). Numerical study of nSi and nSiGe solar cells: Emerging microstructure nSiGe cell achieved the highest 8.55% efficiency. *Optical Materials*, *129*(June), 6. https://doi.org/10.1016/j.optmat.2022.112539

Heo, J. H., Han, H. J., Kim, D., Ahn, T. K., & Im, S. H. (2015). Hysteresis-less inverted CH3NH3PbI3 planar perovskite hybrid solar cells with 18.1% power conversion efficiency. *Energy and Environmental Science*, *8*(5), 1602–1608. https://doi.org/10.1039/c5ee00120j

Hosseini, Z., & Ghanbari, T. (2018). Designing an efficient graphene quantum dot-filled luminescent down shifting layer to improve the stability and efficiency of perovskite solar cells by simple optical modeling. *RSC Advances*, *8*(55), 31502–31509. https://doi.org/10.1039/c8ra06196c

Jamal, M. S., Shahahmadi, S. A., Chelvanathan, P., Asim, N., Misran, H., Hossain, M. I., Amin, N., Sopian, K., & Akhtaruzzaman, M. (2019). Effect of defect density and energy level mismatch on the performance of perovskite solar cells by numerical simulation. *Optik*, *182*, 1204–1210. https://doi.org/10.1016/j.ijleo.2018.12.163

Mazumdar, S., Zhao, Y., & Zhang, X. (2021). Stability of Perovskite Solar Cells: Degradation Mechanisms and Remedies. *Frontiers in Electronics*, *2*(August), 1–34. https://doi.org/10.3389/felec.2021.712785

Mohanty, I., Mangal, S., Jana, S., & Singh, U. P. (2019). Stability factors of perovskite (CH3NH3PbI3) thinfilms for solar cell applications: A study. *Materials Today: Proceedings*, *39*(July 2021), 1829–1832. https://doi.org/10.1016/j.matpr.2020.06.183

Sabbah, H., Arayro, J., & Mezher, R. (2022). Simulation and Investigation of 26% Efficient and Robust Inverted Planar Perovskite Solar Cells Based on GA0.2FA0.78SnI3-1%EDAI2 Films. *Nanomaterials*, *12*(21), 1–19. https://doi.org/10.3390/nano12213885

Verschraegen, J., & Burgelman, M. (2007). Numerical modeling of intra-band tunneling for heterojunction solar cells in scaps. *Thin Solid Films*, *515*(15 SPEC. ISS.), 6276–6279. https://doi.org/10.1016/j.tsf.2006.12.049

Vivaldo, I., Carrillo, J., López, O., Jiménez, S., Martínez, J., Murias, D., & López, J. A. (2016). Study of the photon down-conversion effect produced by thin silicon-rich oxide films on silicon solar cells. *INTERNATIONAL JOURNAL OF ENERGY RESEARCH*, *33*(4), 23–40. https://doi.org/10.1002/er

Yang, J., Luo, X., Zhou, Y., Li, Y., Qiu, Q., & Xie, T. (2022). Recent Advances in Inverted Perovskite Solar Cells: Designing and Fabrication. *International Journal of Molecular Sciences*, *23*(19). https://doi.org/10.3390/ijms231911792

Yin, Z., Lu, B., Chen, Y., & Guo, C. (2022). Advances of Commercial and Biological Materials for Electron Transport Layers in Biological Applications. *Frontiers in Bioengineering and Biotechnology*, *10*(May), 1–20. https://doi.org/10.3389/fbioe.2022.900269

ISSN 2523-2881

Article **Journal Renewable Energy**
June, 2023 Vol.7 No.18 9-18

Low-cost Schlieren system for flow visualization in transparent media in the wind sector

Sistema Schlieren de bajo costo para visualización de flujos en medios transparentes en el sector eólico

URIBE-CASTILLO, Citlali† & RICO-ESPINO, José Guadalupe*

Universidad Tecnológica de Querétaro, División Ambiental, Área de Energías Renovables

ID 1st Author: *Citlali, Uribe-Castillo* / **ORC ID:** 0009-0009-3832-8654, **CVU CONAHCYT ID:** 1292854

ID 1st Co-author: *José Guadalupe, Rico-Espino* / **ORC ID:** 0000-0001-9371-0885**, CONAHCYT ID:** 208880

DOI: 10.35429/JRE.2023.18.7.9.18 Received March 30, 2023; Accepted June 30, 2023

Abstract

The Schlieren technique is frequently used for qualitative visualization of flow around an object. Temperature and density change can also be obtained with this technique. In this project, the aim was to develop a low-cost Schlieren system starting from easily available materials and commercial equipment. Cell phone holders were used as supports to position the concave mirrors. A light-emitting diode (LED) lamp was used as the illumination source, while a knife, a condenser lens, and printed parts in PLA (polylactic acid) plastic were key to the prototype development. Preliminary results showed an effect with limited visual perception due to the low temperature change in the objects under examination. In later experiments, qualitative visualization with a better degree of visual perception was observed due to the higher temperature range reached in the test. The images that were obtained were satisfactory and they allowed validation of the prototype development. Its main application points to the visualization of transparent flows that are formed in the airfoil of a wind turbine blade.

Schlieren, Flow, Blade, Aerodynamic airfoil

Resumen

La técnica Schlieren se utiliza con frecuencia para la visualización cualitativa del flujo que envuelve un objeto. Los cambios de temperatura y densidad pueden ser obtenidos también con esta técnica. En este proyecto el objetivo es el desarrollado de un sistema Schlieren de bajo costo, a partir de materiales y equipos comerciales de fácil acceso. Para posicionar los espejos cóncavos se usaron soportes del tipo para teléfono celular. Una lámpara con un diodo emisor de luz (LED) como fuente de iluminación, una navaja, una lente condensadora y piezas impresas en plástico PLA(ácido poliláctico), fueron la clave en el desarrollo del prototipo. Los primeros resultados mostraron un efecto con escasa percepción visual debido a la baja variación de temperatura en los objetos de prueba. En los resultados finales se realizaron visualizaciones cualitativas con mejor grado de percepción visual debido al rango de temperatura más elevado alcanzado en las pruebas. Las imágenes obtenidas fueron adecuadas y permitieron validar el prototipo desarrollado. Su aplicación principal se orienta en la visualización de los flujos transparentes que se forman en el perfil aerodinámico de un alabe de un aerogenerador.

Schlieren, Flujo, Alabe, Perfil aerodinámico

Citation: URIBE-CASTILLO, Citlali & RICO-ESPINO, José Guadalupe. Low-cost Schlieren system for flow visualization in transparent media in the wind sector. Journal Renewable Energy. 2023. 7-18: 9-18

*Correspondence to Author (e-mail: jose.rico@ciateq.mx)
† Researcher contributing as first author.

I. Introduction

Wind turbines use the force of the wind to produce electrical energy by converting kinetic energy into mechanical energy. In Mexico, there are only nine wind energy-producing states. Oaxaca is the main generator and in 2021 it provided 2,749 MW, which is equivalent to 10% of the country's total production. The states of Tamaulipas, Jalisco, Nuevo León, Chiapas, Baja California, San Luis Potosí, Sonora, and Quintana Roo also have wind power plants with a lower production percentage. (Fernández, 2023)

The blades of a wind turbine are one of its main components. They are designed to have a life cycle of approximately 20 years, during which time they will be subjected to extreme loads and fatigue due to the action of the wind and therefore they will become increasingly susceptible to instabilities caused by these phenomena. These loads cause vibrations in the wind turbine, and premature failures or wear appear in its components, causing low efficiency in energy production, costs, and lifetime of the system.(Vicente Ramírez, 2021)

The trend for wind turbine development and innovation is to search for more adaptable structures and materials, due to the need to reduce mass. However, by doing so, turbines are exposed to more vibrations and, therefore, to the generation of failures in their components. As a result, there are inevitable losses in energy production.

The purpose of this research is to apply a qualitative technique that allows visualizing the flows formed around the blade of a wind turbine. In order to observe this phenomenon, the Schlieren technique will be applied. This is an optical technique to visualize flow with density changes, from which information is obtained about flow variables, such as the different densities along a section. A light source, two parabolic mirrors, a blade, and a screen or image sensor are needed to assemble the system. The system has a "Z" configuration, with the test area in the center.

In this study, a low-cost system is proposed, which allows the visualization of flows in transparent media in the blade of a wind turbine by means of qualitative analysis that allows its implementation and academic use.

II. Resources used

For the development of the prototype, several resources were used. The total assembly cost was approximately US$1,000. Including direct costs (tools and materials) and indirect costs (services and special equipment).

III. Development

This section describes the methodology that was applied to develop the prototype of the Schlieren System. Firstly, the state of the art of the Schlieren technique is presented to introduce background information on previous works. Secondly, the design of the components by a CAD software is shown, which was used to make the necessary parts for the system structure. Finally, the development and assembly of the system is reported.

Background

The Schlieren effect is the set of non-homogeneities of a transparent material, not visible to the human eye. The study of this effect began when the need arose to develop high-quality lenses that did not present these inhomogeneities. The father of inhomogeneous media optics was the scientist Robert Hooke. He observed the Schlieren effect in 1665 with a system consisting of a large convex lens and two candles, as shown in Figure 1. One candle served as the light source, and the other produced the rising hot air, which he observed with his system. He was probably the first scientist to use a Schlieren-type setup, aiming to visualize the different densities produced by combustion. Unfortunately, his method was not precise enough to obtain optimal results. (Settles, 2001)

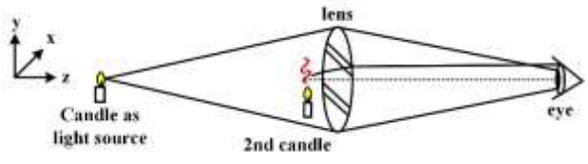

Figure 1 Hooke's optical configuration, with two candles, a lens, and a human eye
Source: Own Elaboration

ISSN 2523-2881

The Dutch astronomer Christiaan Huygens also designed a Schlieren system for the detection of irregularities in lenses, which consisted of a distant light source focused on the lens to be studied resulting in an image of varying brightness, which indicates the original irregularities of the lens.

August Toepler adapted the Schlieren for flow visualization, developed from the Foucault knife configuration, which resulted in improved quality, contrast, and sensitivity of Schlieren images compared to images obtained with previous arrangements.

Propagation of light in a homogeneous medium

The Schlieren technique is used to determine flow density gradients in fluids by observing refraction as light goes through these gradients, so it is necessary to find a relationship between the refractive index of the medium and the density of the medium. The following equation can be used:

$$n - 1 = k \cdot \rho \quad (1)$$

where n and ρ are the refractive index and density of the medium, respectively, and *k* is the Gladstone-Dale Constant, which is a function of the particular gas and the wavelength of light used in the optical system.

The refractivity $(n - 1)$ of a gas depends on gas composition, temperature, density, and wavelength of illumination. In many cases, the temperature, density, and pressure of gases not far from normal atmospheric conditions are more closely related to the simple equation of state of the perfect gas:

$$\frac{p}{\rho} = R \cdot T \quad (2)$$

where *R* is the specific gas constant, *T* is temperature, ρ is density and *p* is pressure. Gases flowing with varying density are called compressible flows and they may arise due to temperature differences or high gas velocities. All these conditions may lead to perturbations of gases that refract light, which can be visualized by refraction changes.

Definition of the Schlieren System

The optical system or Schlieren photography is an optical technique in which the variation of the density gradient of a transparent, inhomogeneous medium is observed. This technique can be applied both to liquids and solids. Changes in density, or refractive index, can be due to different factors such as temperature change, exposure to high-velocity flows, and the presence of particles that do not belong to the material under study.

This technique is used to visualize aerodynamic flows and in quality control systems for crystals, glasses, and optical elements. (Gómez González, 2006)

Conceptual design of Z-array

Z-type Schlieren mirror array: Its name refers to its geometry which consists of two parabolic mirrors in series and the test zone between the two mirrors, as shown in Figure 2. The light source located at the focal distance of the first mirror projects the light over the entire surface of the mirror, it reflects and collimates it in the direction of the second mirror, and then it concentrates it on the knife, located at the focal distance of the second mirror. Finally, the camera is placed behind the knife. (Balduzzi & Balduzzi, 2020)

Z-type 2-mirror Schlieren system: Spherical, parabolic, and concave off-axis mirrors are often used as Schlieren equipment. However, the most popular arrangement is by far the Herschellian Z-type system that uses two parabolic mirrors on oppositely tilted axes. The combination of a diverging light beam, and an opposing converging analyzer beam, and a parallel beam between the two mirrors forms the letter Z, hence the name.

This system is currently the most widely used due to the large space created for testing and the optimal results achieved. However, it requires precise calibration, and its design must minimize optical aberrations arising from non-alignment of all components.

ISSN 2523-2881

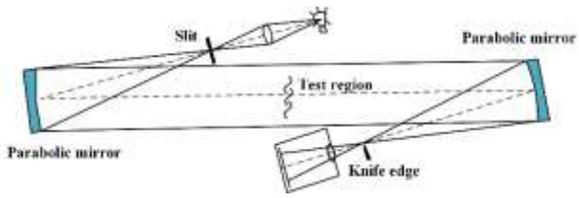

Figure 2 Schlieren Z-type system
Source: Own Elaboration

Distribution

The structuring of each part of the Type Z system, as shown in Figure 3, should be focused on decreasing optical aberrations (coma and astigmatism) and establishing sufficient space for object localization.

– The light source should be placed at the focal length (f_1) of the Mirror 1, to collimate the light beam with an angle of incidence equal to twice the compensation angle (θ_1) of Mirror 1. The compensation angle is the angle of rotation of the mirror in the XZ-Plane with respect to the vertical, or Y-Axis.

Compensation angle $= \theta_1 = \theta_2 = \theta$;

Angle of incidence $= 2\theta_1 = 2\theta_2 = 2\theta$;

The two parabolic mirrors used must be equal, so:

– Mirror 1 focal length (f_1) = Mirror 2 focal length $(f_2) = f$;

– The light beam is reflected and collimated by Mirror 1 towards Mirror 2, which must be placed in alignment with the optical axis and at a minimum of twice the focal length 2*f*, to have enough space for testing.

– Mirror 2, which has an angle of compensation equal to Mirror 1 but in the opposite direction, reflects the beam towards the knife, which is placed at a distance equal to the focal length, f.

– Finally, the camera is positioned after the knife at a distance depending on the used set of lenses, trying not to exceed 10 cm between the knife and the camera sensor. (Rosas Bonilla, 2018)

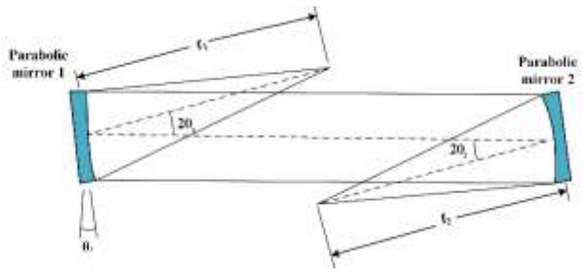

Figure 3 Schlieren system assembly: type Z distribution
Source: Own Elaboration

Sensitivity

The sensitivity of a measuring instrument is one of its basic characteristics, relating the output of the instrument to the received input. This technique is very sensitive to deviations of the incident light beam, allowing changes in density or refractive index to be visualized.

Previous work

In this project, research was conducted on some articles that served as a reference for the design of a low-cost Schlieren system.

Kinsman (Kinsman, 2020) developed a design for a system that any student could build, align, and experiment with. This simple design uses a plastic Fresnel lens found in projectors.

Similarly, Stein (Stein, 2022) presented a system based on a single-mirror configuration, with a smartphone as the light source and the smartphone camera as the detector. The construction of the Schlieren Imaging System for smartphones is simple and affordable, and all parts used are 3D printable.

Additionally, research that used Schlieren images is presented in the work by Zhang (Zhang *et al*., 2023) , focused on supersonic viewing tunnels, and Doroshchenko (Doroshchenko, 2023) , about processing and analysis of Schlieren images. Other Schlieren visualization techniques, such as the Synthetic type, were developed by Li and Xu (Li & Xu, 2023).

ISSN 2523-2881

Mechanical Design

The first step to building the Schlieren System was to design it in the SolidWorks© program (Dassault Systèmes, 2023). The objective of the mechanical design is that the system should be as aligned as possible because the focal point must coincide with the two mirrors, the camera, and the lamp; the result is an image of flow visualization. The Schlieren System that was developed had a Z-arrangement, as shown in Figure 4.

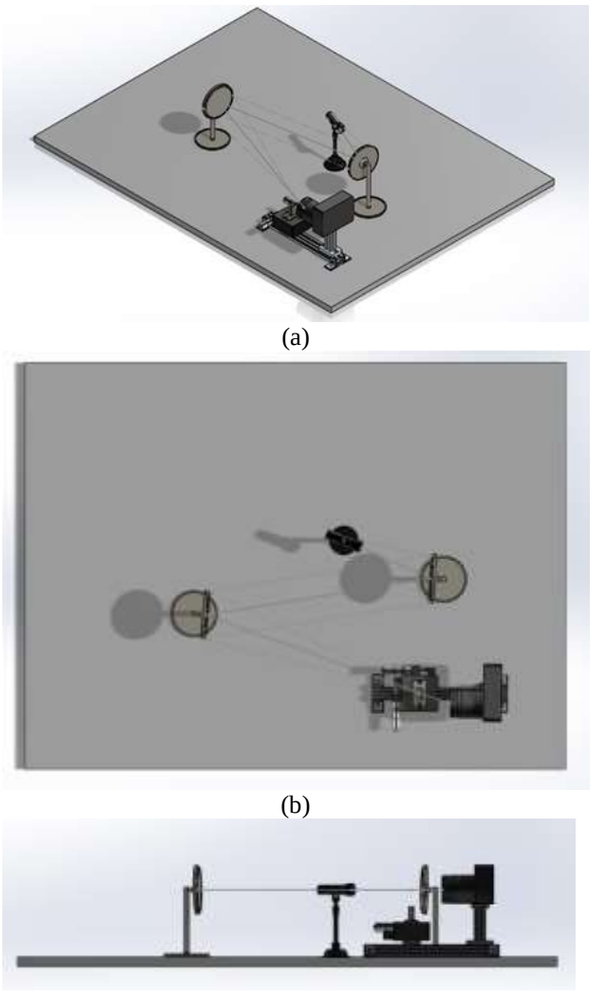

(a)

(b)

(c)

Figure 4 Schematic of Schlieren System Z-array: (a) isometric view, (b) top view, (c) front view
Source: Own Elaboration

The mechanical design and distribution of the components in a virtual environment allow validating their position and the quantity of materials to be used.

Physical assembly of the Schlieren System

The whole system was assembled with the designed components, as shown in Figure 5. At this stage, the alignment of the main elements was adjusted.

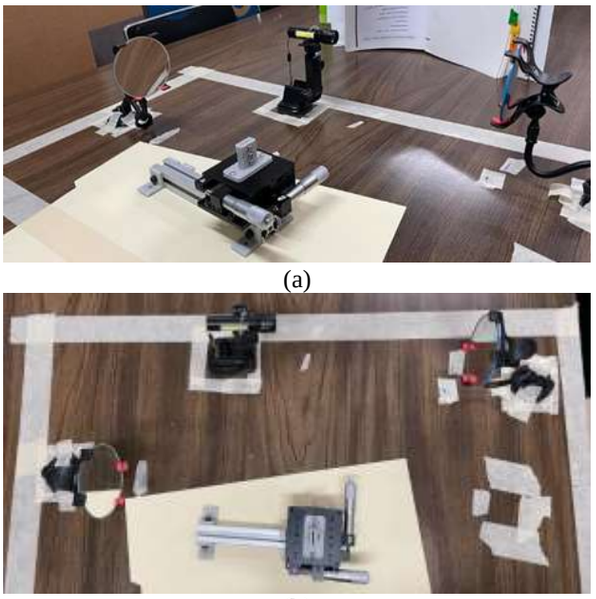

(a)

(b)

Figure 5 Assembly of the Schlieren System: (a) lateral view, (b) top view
Source: Own Elaboration

Blade segment of a wind turbine

A blade segment of the wind turbine was 3D-printed with PLA material. The design was created with the SolidWorks© program and it is shown in Figure 6 (Dassault Systèmes, 2023).

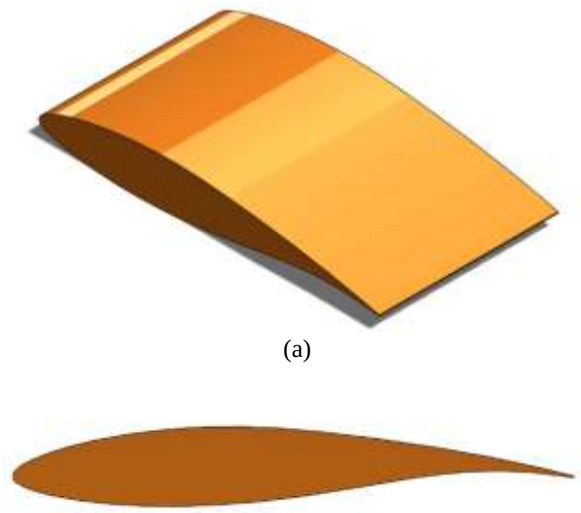

(a)

(b)

Figure 6 Blade segment (a) isometric and (b) front view
Source: Own Elaboration

ISSN 2523-2881

Modification and improvements to the Schlieren System

The first results obtained were not entirely satisfactory, because the Schlieren effect could not be observed in the performed tests. Therefore, it was decided to make various adjustments to the Schlieren system, such as adding a condenser lens, to concentrate the light of the lamp, and direct it towards the mirror. Additionally, the arrangement was modified, as shown in Figure 7. The adjusted distribution includes the condenser lens.

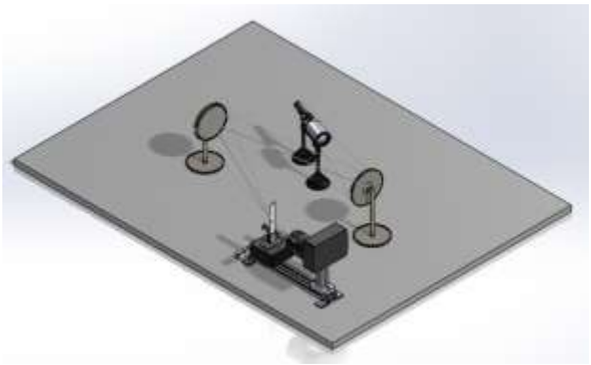

(a)

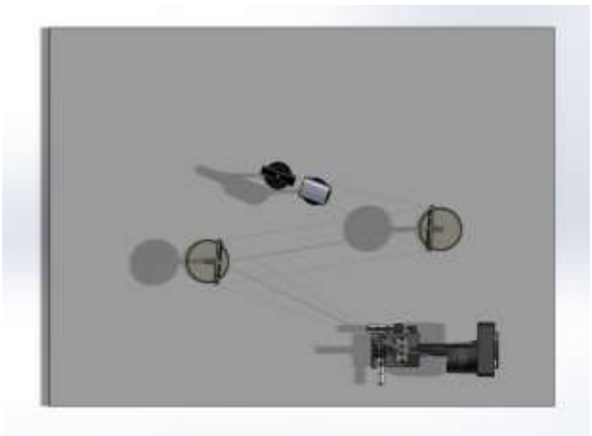

(b)

(c)

Figure 7 Schlieren system with condenser lens: (a) isometric view, (b) top view, (c) front view. *Source: Own Elaboration*

Schlieren system

The final Schlieren System is shown in Figure 8. A sketch of the Schlieren system (Figure 9) as well as the measurements of its orientation angles and the distance at which each mirror should be placed (Figure 10) were also prepared as a reference for future installations so that it could be assembled anywhere. The next stage was testing the system behavior.

Figure 8 Final Schlieren system
Source: Own Elaboration

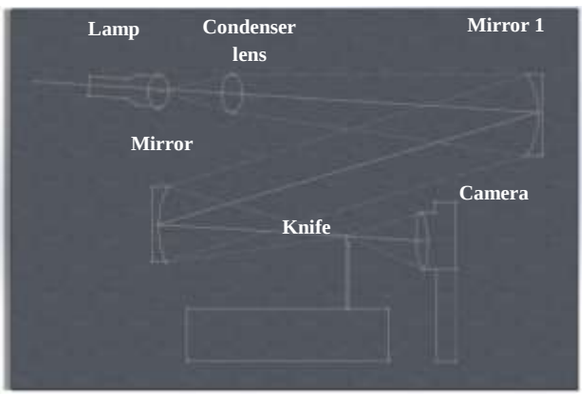

Figure 9 Schlieren system sketch
Source: Own Elaboration

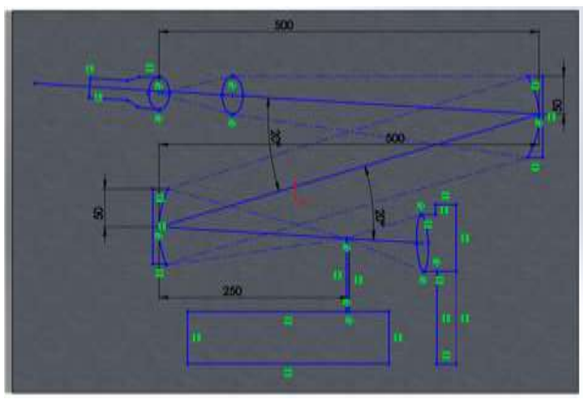

Figure 10 Schlieren system sketch with dimensions
Source: Own Elaboration

ISSN 2523-2881

IV. Experimentation

Preliminary tests were carried out with a hot air gun reaching a temperature of 60°C. These tests were not entirely satisfactory since the effect could not be appreciated because the variation of the refractive index with the temperature was not sufficient to be appreciated in the system.

Subsequently, other tests were carried out using an air gun with higher temperature and another one with solid alcohol. In this case, satisfactory results were obtained since the Schlieren effect could be observed, as shown by comparing Figure 11 and Figure 12.

Figure 11. Preliminary test with air gun
Source: Own Elaboration

Figure 12 Test with solid alcohol
Source: Own Elaboration

After obtaining the results of the tests performed on the Schlieren system for qualitative visualization of the phenomenon in transparent flows, in a subsequent stage, further application of both qualitative and quantitative visualization can be obtained from a blade segment. Quantitatively, the blade exit zone can be instrumented using strain gauges. In this area vibrations occur at the angles of attack where the wind flow changes from laminar to turbulent.

The process of gluing strain gauges is shown in Figure 13 and Figure 14. Four points were instrumented: two each in the low-pressure and high-pressure zone (top and bottom surface).

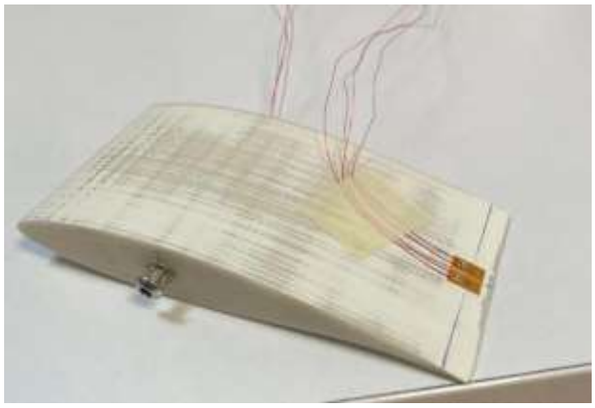

Figure 13 Strain gauges positioned on the top surface
Source: Own Elaboration

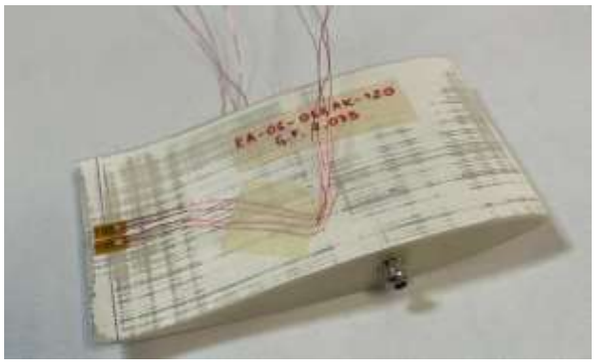

Figure 14 Strain gauges fixed at the bottom surface
Source: Own Elaboration

V. Analysis of results

The purpose of this section is the analysis and interpretation of the results obtained from the Schlieren system. The information is presented as a sequence of images.

In the images captured from the test performed with solid alcohol (Figure 15), it can be seen that flow visualization is clearer than with the hot air gun (Figure 16).

ISSN 2523-2881

This is due to the solid alcohol reaching a higher temperature than the hot air gun, which reaches a maximum temperature of 60°C, and, therefore, the phenomenon can be better appreciated. On the other hand, it should also be mentioned that the system is not as sensitive as expected, since there should be no problem when performing tests, even at lower temperature. Preliminary analysis indicates that the increase in temperature between a hot air gun and the solid alcohol flame allows a significant change in air density. Therefore, the refractive index also undergoes a considerable change that is sufficient for the Schlieren System to be able to detect it.

Figure 15 Sequence of Schlieren images captured in the solid alcohol test
Source: Own Elaboration

Figure 16 Sequence of Schlieren images captured in the air gun test
Source: Own Elaboration

A promising improvement adopted after the preliminary tests was to modify the bases of mirrors and lamp. The bases were printed in PLA material so that the system could be installed and transported anywhere, in addition to increasing the aesthetics of the prototype. Figure 17 shows the new design of the bases supporting the concave mirrors that allowed better adjustment.

Figure 17 New bases for the Schlieren system
Source: Own Elaboration

VI. Conclusions

The objective of this project was to develop a prototype for flow observation in transparent media. Among the different Schlieren configurations available, the Schlieren Z-array technique was selected.

This technique was the most efficient for the observation of the phenomenon since it has a wider space to perform the tests and, due to light refraction, it can reduce one of the optical aberrations that in this type of system, in this case, astigmatism.

In this project, special care was given to the design and assembly arrangement that were created in SolidWorks© (Dassault Systèmes, 2023). The manufacturing of the actual parts for the assembly was outsourced. It was necessary to economize by using materials and tools that were available, as well as by planning the design of each piece to reduce the amount to be used. Although the surface finish of the mirrors was not completely smooth, it was possible to meet the expectations and objective for which it was planned.

Improvements to the Schlieren System

Possible improvements and modifications to the system would be to utilize better quality mirrors since the ones that were used here caused some complications at the time of testing and produced blurry images.

VII. Funding

This work has been funded by CIATEQ, A.C. under project number: PQDG12002.

VIII. References

Balduzzi, N., & Balduzzi, N. (2020). *Diseño y construcción de un túnel de viento supersónico con sistema de visualización Schlieren.* [Universidad Nacional de La Plata]. https://repositoriosdigitales.mincyt.gob.ar/vufind/Record/SEDICI_1a1a5472d4057db6451753ca42224a62. oai:sedici.unlp.edu.ar:10915/137588

Dassault Systèmes. (2023). *SOLIDWORKS.* https://www.solidworks.com/es

Doroshchenko, I. A. (2023). Analysis of the experimental flow shadowgraph images by computer vision methods. *Numerical Methods and Programming (Vychislitel'nye Metody i Programmirovanie), 24*(2), 231–242. https://doi.org/10.26089/NUMMET.V24R217

Fernández, L. (2023, April 19). *Installed wind power capacity in Mexico 2011-2022.* https://www.statista.com/statistics/790712/installed-capacity-of-wind-power-generation-mexico/

Gómez González, E. (2006). *Guía básica de conceptos de óptica geométrica.* https://docplayer.es/6274832-Guia-basica-de-conceptos-de-optica-geometrica.html

Kinsman, T. (2020, January 18). *A Simple and Inexpensive Schlieren Optical System Using a Fresnel Lens | PetaPixel.* https://petapixel.com/2020/01/18/a-simple-and-inexpensive-schlieren-optical-system-using-a-fresnel-lens/

Li, H., & Xu, D. (2023). Extended-resolution of a single-camera synthetic Schlieren method for measurement of free liquid surfaces. *Experimental Thermal and Fluid Science*, *149*, 110998. https://doi.org/10.1016/J.EXPTHERMFLUSCI.2023.110998

Rosas Bonilla, B. A. (2018). *Diseño y construcción de técnica de visualizacion de fluidos de alta velocidad Schlieren tipo-Z.* [Fundación Universitaria Los Libertadores]. https://repository.libertadores.edu.co/bitstream/handle/11371/1778/rosas_brayan_2018.pdf?sequence=1

Settles, G. S. (2001). *Schlieren and Shadowgraph Techniques: Visualizing Phenomena in Transparent Media.* (Springer Science & Business Media, Ed.). https://books.google.com.mx/books/about/Schlieren_and_Shadowgraph_Techniques.html?id=HWtB2R0gWFgC&redir_esc=y

Stein, K. R. (2022, June 26). A Low-Cost, Portable, Smartphone Schlieren Imaging System. *Annual Conference Excellence Througn Diversity*.

Vicente Ramírez, J. C. (2021). *Análisis de las vibraciones mecánicas generadas debido al movimiento giroscópico del rotor de un aerogenerador de baja potencia.* [Universidad del Istmo]. http://www.unistmo.edu.mx/bibliotecas/tesis_posgrado/2018-2020/tesis%20Juan%20Carlos%20Vicente%20Ram%C3%ADrez.pdf

Zhang, X., Li, D., Zhang, Z., Huang, B., Wang, R., Pu, H., Huang, Z., & Chen, Z. (2023). Density field measurement deflectometry for supersonic wind tunnels. *Optics Letters*, *48*(7), 1714. https://doi.org/10.1364/OL.485063

ISSN 2523-2881

Article **Journal Renewable Energy**
June, 2023 Vol.7 No.18 19-24

Effect of dye on the efficiency of Grätzel cells

Efecto del colorante en la eficiencia de celdas Grätzel

BERNAL-MARTINEZ, Guillermo[1], MONTES-GUTIERREZ, Jorge*[2,3], GARCIA-GUTIERREZ, Rafael[3] and CONTRERAS-LOPEZ, Oscar[2]

[1]*Centro de Investigación Científica y de Educación Superior de Ensenada, Ensenada, B.C., 22860, México.*
[2] *Universidad Nacional Autónoma de México, Centro de Nanociencias y Nanotecnología. Ensenada, B.C., 22860, México.*
[3]*Departamento de Investigación en Física. Universidad de Sonora. Rosales y Luis Encinas, Hermosillo, Sonora, 83000, México*

ID 1st Author: *Guillermo, Bernal-Martínez* / **ORC ID:** 0009-0001-8148-1832, **CVU CONAHCYT ID**: 993056

ID 1st Co-author: *Jorge, Montes-Gutiérrez* / **ORC ID:** 0000-0002-3078-6548, **CVU CONAHCYT ID**: 387879

ID 2nd Co-author: *Rafael, García-Gutiérrez* / **ORC ID:** 0000-0001-5030-326X

ID 3rd Co-author: *Oscar, Contreras-López* / **ORC ID:** 0000-0003-1463-8606

DOI: 10.35429/JRE.2023.18.7.19.24 Received March 30, 2023; Accepted June 30, 2023

Abstract

Renewable energies are playing a critical role in reducing emissions in the energy generation sector. Photovoltaic technologies have reduced their cost due to the improvements in conversion efficiency, the cost of the materials, the economies of scale, and the investments made in research and development in the private and public sectors. The Grätzel cells are part of the third generation of photovoltaics. This generation of photovoltaics looks to achieve photovoltaic devices with great efficiency while keeping low costs using thin layer processes and non-toxic materials. One of the main features of these solar cells, also known as dye-sensitized solar cells (DSSCs), is that the spectrum of absorbed light depends on the dye used and can be tuned, which have a big effect on the performance of the cell. This feature grants this device great versatility, which gives this technology a great potential to give energy to devices in indoor illumination and as Building Integrated Photovoltaics (BIPV). The relevance and working principle of the Grätzel cells are presented in this text, as well as the steps that were required to build these solar cells in a laboratory setting.

DSSC, Solar energy, Grätzel cells

Resumen

Las energías renovables están desempeñando un papel fundamental en la reducción de emisiones en el sector de la generación de energía. Las tecnologías fotovoltaicas han reducido su coste gracias a las mejoras en la eficiencia de conversión, el coste de los materiales, las economías de escala y las inversiones realizadas en investigación y desarrollo en los sectores privado y público. Las células de Grätzel forman parte de la tercera generación fotovoltaica. Esta generación de fotovoltaica busca conseguir dispositivos fotovoltaicos de gran eficiencia manteniendo bajos costes mediante procesos de capa fina y materiales no tóxicos. Una de las principales características de estas células solares, también conocidas como células solares sensibilizadas por colorante (DSSC), es que el espectro de luz absorbida depende del colorante utilizado y puede sintonizarse, lo que tiene un gran efecto en el rendimiento de la célula. Esta característica otorga a este dispositivo una gran versatilidad, lo que confiere a esta tecnología un gran potencial para dar energía a dispositivos en iluminación interior y como Fotovoltaica Integrada en Edificios (BIPV). En este texto se presentan la relevancia y el principio de funcionamiento de las células de Grätzel, así como los pasos que fueron necesarios para construir estas células solares en un entorno de laboratorio.

DSSC, energía solar, células de Grätzel

Citation: BERNAL-MARTINEZ, Guillermo, MONTES-GUTIERREZ, Jorge, GARCIA-GUTIERREZ, Rafael and CONTRERAS-LOPEZ, Oscar. Effect of dye on the efficiency of Grätzel cells. Journal Renewable Energy. 2023. 7-18: 19-24

† Researcher contributing as first author.

Introduction

The use of renewable energy and solar cells have taken a leading role in the shift towards cleaner generation sources [1]. The manufacturing of photovoltaic solar cells has decreased significantly in cost due to the great investment of the public and private sectors in innovation. Silicon photovoltaic cells also have a series of disadvantages, such as the high price of extracting the silicon necessary for the cells or the use of a limited fraction of the electromagnetic spectrum.

One of the alternatives to this type of cells are the Grätzel cells or dye-sensitized solar cells (DSSCs), which present very interesting characteristics such as: low production cost, selection of a specific absorption range, there are light and semi-transparent [2]. Moreover, these characteristics are of interest for their application in the architecture of buildings [3], electronic devices [4], terrestrial storage [5], and portable generation devices [6].

DSSCs are a type of third-generation solar cell that differs from other types of solar cells in that the charge carrier generation and the transport mechanism occur at different sites [7]. These cells perform outstandingly in other interiors, and it could take advantage of artificial light compared to solar cell technologies. This is one of the essential advantages that DSSCs have in relation to other photovoltaic cell technologies. For example, the Internet of Things (IoT), technology that aims to connect all kinds of electronic devices, sensors, wearable devices, and smart meters through wireless connections [8].

Even though many smart devices are connected with communication networks, there are significant problems in providing electricity to such devices. For IoT devices, batteries are usually the power sources, however, the disadvantage of using batteries is that their lifetime is limited to months or years. Also, the power required for IoT devices is typically low and can be supplied under indoor lighting conditions using DSSC. Therefore, indoor DSSCs are considered as promising systems for power supply to IoT devices [9-10].

Constitution, characteristics, and operation of a DSSC

A DSSC is represented as a tandem by superimposing nanocrystalline semiconductor films between two electrode substrates (usually both transparent, ITO for example), in the following order the intermediate layers where REDOX reactions are generated to produce electrons are represented: a) mesoporous film (photoanode) sensitized with the dye, b) electrolyte solution and c) a catalyst, which covers a conductive substrate (counter electrode) (see figure 1).

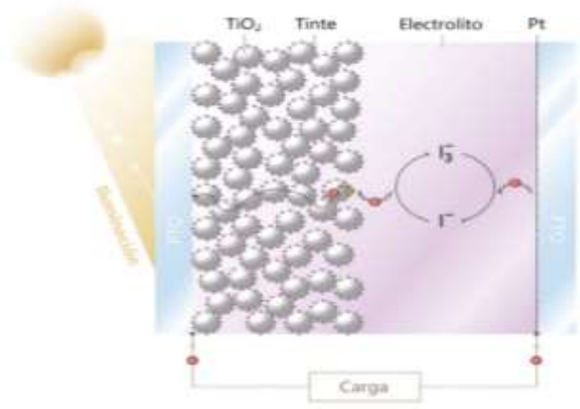

Figure 1 Operating principle of a Grätzel cell [11]

The operation of the DSSC's occurs when electrons are produced from the light that passes through the transparent conductor and interacts with a dye, which is supported on a mesoporous layer of semiconductor nanoparticles (2-15 μm thick and 10-30 nm in diameter, usually TiO_2). When light interacts with the dye, a portion of the light is absorbed and shifts a portion of the dye's electrons to a higher energy state (bringing the dye to its S* excited state).

Consequently, these electrons can be used if they are injected into the mesoporous layer or they can be lost through a series of recombination pathways to the dye (10-4 s), to the electrolyte (10-2 s) or the decay of the dye to its ground state (10- 9s). The electrolyte is a layer or medium that facilitates charge transport to the anode (I-/I-3 dissolved in acetonitrile is usually used) [12].

ISSN 2523-2881

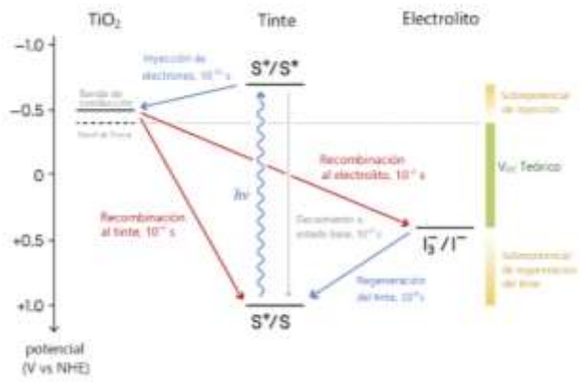

Figure 2 Energy diagram of a Grätzel cell [9].

Methodology

For the assembly of the DSSC's, glass slides were used and a layer of ITO (250nm, 70-100 Ω /cm2) was deposited for the top electrode (cathode) and for the bottom electrode (anode) a layer of ITO (250 nm, 70-100 Ω/cm2) + Pt (50 nm) (ITO was deposited by sputtering and Pt by e-beam evaporation). Next, the assembly of the DSSC's cells is described in 4 steps:

1. A layer of TiO_2 NP's was deposited on the top electrode from 100 µl of a solution of 2 g TiO_2 NP's + 0.05 g of PEG + 0.5 ml of Triton X-100 in 6 ml of 1M HNO3.
2. The top electrode (glass+ITO+ TiO_2 NP's) was heated to 80°C and immersed in the dye for 24 hours and allowed to dry at room temperature.
3. The surface of TiO_2 NP's + dye of the top electrode was impregnated by dripping with a solution of 0.5M Potassium Iodide + 0.05M Ethylene Glycol Iodide.
4. The previously activated bottom electrode was placed at 400°C for 15 min.

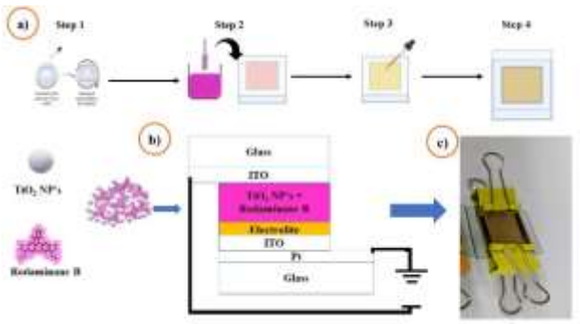

Figure 3 DSSC's assembly diagram. a) shows 4 steps to assemble the DSSC's, b) diagram of the DSSC model and c) DSSC assembled in the laboratory

Results and Discussion

In the present work, the open circuit voltage (Voc), electrical current density (Jsc), conversion efficiency (η) and form factor or fill factor (FF) associated with the composition of the DSSC were analyzed. Cells with upper electrode of Pt NP´s deposited by deep coating, Pt film by sputter deposition, the TiO_2 layer by the Dr. Blade method, TiO_2 by spin coating and the types of dye: Rhodamine B and Anthocyanin, were compared. (See table 1).

Variable	A)	Parameters	B)	Parameters
Pt	Deep coating	10 seconds and dry by 5 minutes.	Sputtering	25sccm of Ar, 3 mTorrs and 8% power of DC source
TiO_2	Deep coating	Mascaraed	Spin coating	3000 rpm by 40 seconds
Dye	Rhodamine B	80°C by 24 hours	Anthocyanin	80°C by 24 hours

Table 1 Variables compared in the manufacture of DSSC's cells

After two hours of stirring a colloidal solution of 2 g of TiO_2 NPs in 96 ml of methanol and 4 ml of 0.1 M nitric acid; ITO/Glass is dipped. Figure 4 shows the result of the deposit by the dip coating method of the mesoporous layer made up of TiO_2 NPs on a glass-supported ITO film. In c) a pair of micrographs taken in an optical microscope of the TiO_2 layer with a very uniform appearance is observed, and in d) the roughness of the surface between 1 µm and 3 µm is observed by AFM with scans of 15µm x 15µm.

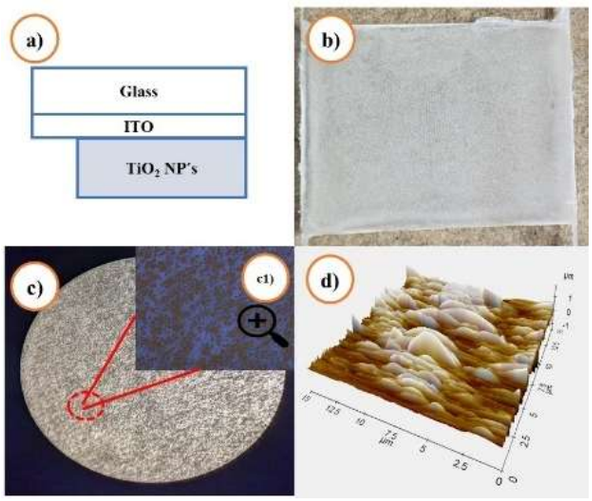

Figure 4 Deposit by the dip coating method. a) shows top electrode schematic, b) photograph of TiO_2 NP's deposition on a glass-supported ITO film, c) 10X optical micrograph and c1) 50X zoom, and d) NP's surface topography of TiO_2 by AFM of 15µm x 15µm

ISSN 2523-2881

Figure 5 shows the result of the deposit by the spin coating method of the mesoporous layer made up of TiO_2 NPs on a glass-supported ITO film. 100 µl of a solution of 2 g TiO_2 NP's + 0.05 g of PEG + 0.5 ml of Triton X-100 was placed in 6 ml of 1M HNO_3. The equipment was programmed at 3000 rpm for 40 seconds. In c) a micrograph taken in an optical microscope of the TiO_2 layer with a very compact and uniform appearance is observed, and in d) the AFM scan of 35µm x 35µm is observed, a step can be seen with which an average thickness of 7.68 µm.

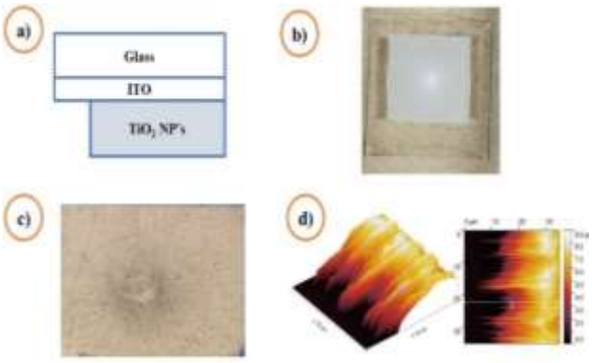

Figure 5 Deposit by the spin coating method. a) shows top electrode schematic, b) photograph of TiO2 NPs deposition on a glass-supported ITO film, c) 10X optical micrograph, and d) surface topography of TiO_2 NPs by 35µm AFM x 35

Figure 6 shows the manufacture of the bottom electrode. For this, it was tested to deposit a layer of Pt NP's and a uniform Pt film by sputter deposition on Glass and later ITO on the Pt NP's/Glass and Ptfilm/Glass correspondingly. In b) a photograph of the ITO/Pt NP's/Glass film with a slightly opaque and translucent appearance is observed. The Pt NP's were synthesized from 134.14 µl of 6.09 mM chloroplatinic acid (H_2PtC_{l6}) in 30 ml of deionized water + 10.75 mg of polyvinylpyrrolidone (PVP) as protective agent + 1 ml of 1% sodium borohydride ($NaBH_4$), 127.5 µl of the Pt NP's solution were added on the Glass and allowed to dry, subsequently heated to 400°C to activate the surface of the Pt NP's. In c) a very uniform Ptfilm/Glass film. The sputter deposition equipment was operated at a DC source power of 8%, Ar gas flow of 25 sccm and 3 mTorrs.

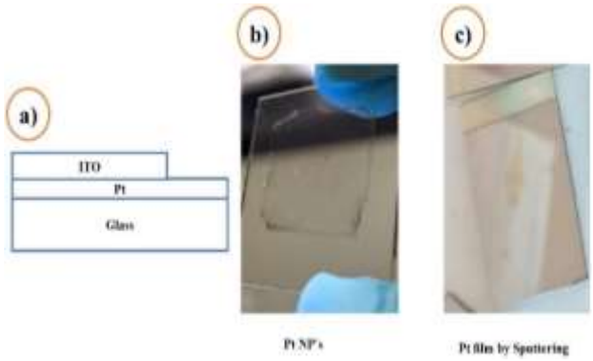

Figure 6 Deposit of the bottom electrode. a) shows diagram of bottom electrode, b) bottom electrode ITO/Pt NP's/Glass, and c) ITO/Ptfilm/Glass

Figure 7 shows the assembly of the DSSC's, in a) the top electrodes of TiO2 NP's/ITO/Glass are prepared, in b) they are subsequently impregnated with the dye, in c) the electrolyte is added, and it is connected to the bottom electrodes of ITO/Pt NP's/Glass and ITO/Ptfilm/Glass (they were fixed with metallic tweezers to avoid movement). In d) a complete schematic of the DSSC´s is observed.

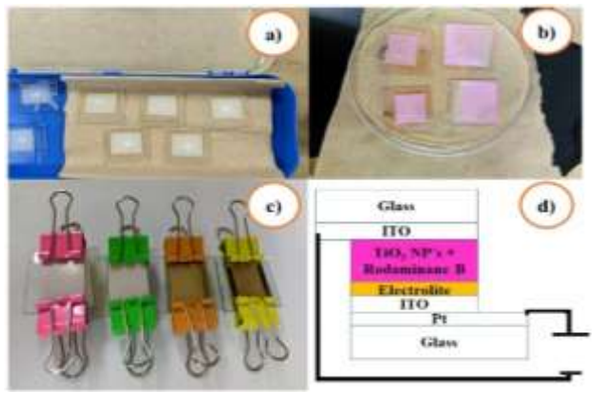

Figure 7 Assembly of the DSSC's. a) TiO2 NP's/ITO/Glass top electrode, b) TiO_2 NP's/ITO/Glass upper electrode + dye, c) top and bottom electrode assembly, d) complete schematic of a DSSC cell

Figure 8 shows the electrical circuit model that allows the measurement of the current and voltage of a solar cell contains a variable resistor, ranging from 3 Ω to 10,000 Ω, which is connected in parallel with the solar cell. For the measurement of the variables, a current meter is placed in series with the cell and the resistance, and a voltage meter is placed in parallel.

ISSN 2523-2881

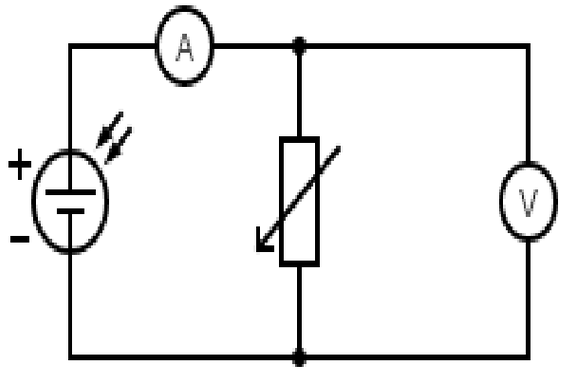

Figure 8 Circuit diagram for the measurement of the electrical variables of the DSSC

In annexes section is the table 2 with variations of solar cells and their measured electrical variables. The table 3 show results about photovoltaic performance of DSSC´s using Rhodamine B and Anthocyanin.

Dye	Jsc (mA/cm^2)	Voc (mV)	Mpp (μW)	FF	η (%)
Rhodamine B	0.02285	505	11.41	0.3043	0.0037
Anthocyanin	0.3812	380	78.8	0.2166	0.0145*

* For the efficiency of the anthocyanin cell 1.5AMG illumination was assumed.

Table 3 Photovoltaic performance of DSSC´s using two different dyes

Conclusions

During the development of the manufacturing of the different cells, methods such as Deep coating were tested, which is a simple and cheap technique, however, when testing the Sputtering process, the results were similar among its variants, uniform on the surface eye and resistant to the manipulation.

All the results with illumination with the Sun show similar values of states of polarization related to Voc (open circuit voltage) and the comparison with illumination under a solar simulator, it presents values twice as high as those with the sun. The values of the current flow Jsc were also observed different in relation to lighting, however, what stands out is the difference between the cells manufactured with Rhodamine B and Anthocyanin, where the latter presents better values in general in relation to efficiency.

Consequently, the results of this work provide a description and comparison of the various methods that offer an excellent alternative for the manufacture of DSSC's cells, and derived from these results many proposals arise to develop innovation in the manufacture of photovoltaic devices (modification of the dye, manufacture of DSSC's devices with microfluidics to vary or exchange the dye, among others) and the versatility of its applications in relation to architecture, ergonomics in work areas in relation to lighting, remote control of DSSC's devices (IoT), among others.

References

[1] REN21. 2019. Renewables 2019 Global status report. Recuperado el 20 de marzo de 2020, a partir de https://core.ac.uk/download/pdf/328806729.pdf

[2] Arjunan, T. v y Senthil, T. S. 2013. Review: Dye sensitised solar cells. Materials Technology. Taylor & Francis, 28(1–2), 9–14. https://doi.org/10.1179/1753555712Y.0000000040

[3] Lamberti, A., Sacco, A., Bianco, S., Giuri, E., Quaglio, M., Chiodoni, A., & Tresso, E. (2011). Microfluidic sealing and housing system for innovative dye-sensitized solar cell architecture. *Microelectronic engineering*, *88*(8), 2308-2310. https://doi.org/10.1016/j.mee.2010.12.114

[4] Ali, N., Hussain, A., Ahmed, R., Wang, M. K., Zhao, C., Haq, B. U., & Fu, Y. Q. (2016). Advances in nanostructured thin film materials for solar cell applications. *Renewable and Sustainable Energy Reviews*, *59*, 726-737. https://doi.org/10.1016/j.rser.2015.12.268

[5] Gong, J., Liang, J., & Sumathy, K. (2012). Review on dye-sensitized solar cells (DSSCs): Fundamental concepts and novel materials. *Renewable and Sustainable Energy Reviews*, *16*(8), 5848-5860. https://doi.org/10.1016/j.rser.2012.04.044

[6] Li, G., Sheng, L., Li, T., Hu, J., Li, P., & Wang, K. (2019). Engineering flexible dye-sensitized solar cells for portable electronics. *solar energy*, *177*, 80-98. https://doi.org/10.1016/j.solener.2018.11.017

ISSN 2523-2881

[7] Zhang, L., Zhang, J., Tang, X., Chen, Y., Wang, X., Deng, Z., ... & Sun, B. (2023). Densely Packed D− π–A Photosensitizers on TiO2 Enable Efficient Dye-Sensitized Solar Cells. *ACS Applied Energy Materials*, *6*(8), 4229-4237. https://doi.org/10.1021/acsaem.3c00072

[8] Aslam, A., Mehmood, U., Arshad, M. H., Ishfaq, A., Zaheer, J., Khan, A. U. H., & Sufyan, M. (2020). Dye-sensitized solar cells (DSSCs) as a potential photovoltaic technology for the self-powered internet of things (IoTs) applications. *Solar Energy*, *207*, 874-892. https://doi.org/10.1016/j.solener.2020.07.029

[9] Devadiga, D., Selvakumar, M., Shetty, P., y Santosh, M. S. (2021). Dye-sensitized solar cell for indoor applications: A mini-review. Journal of Electronic Materials, 50(6), 3187–3206. https://doi.org/10.1007/s11664-021-08854-3

[10] Bifari, E. N., Almeida, P., & El-Shishtawy, R. M. (2023). Advancing Panchromatic Effect for Efficient Sensitization of Cyanine and Hemicyanine-based Dye-Sensitized Solar Cells. *Materials Today Energy*, 101337. https://doi.org/10.1016/j.mtener.2023.101337

[11] Calogero, G., Citro, I., Crupi, C., Carini, G., Arigò, D., Spinella, G., Bartolotta, A., y di Marco, G. (2019). Absorption spectra, thermal analysis, photoelectrochemical characterization and stability test of vegetable-based dye-sensitized solar cells. Optical Materials, 88, 24–29. https://doi.org/10.1016/j.optmat.2018.11.005

[12] Lau, K. K., & Soroush, M. (2019). Overview of dye-sensitized solar cells. *Dye-Sensitized Solar Cells*, 1-49. https://doi.org/10.1016/B978-0-12-814541-8.00001-X

Founding

This project has been founded by CONAHCYT-FORDECyT (FORDECYT-272894); Postdoctoral fellowship (2021 and 2022, CVU 387879); and Núcleo de Investigación Científica y de Desarrollo Tecnológico for the use of the facilities.

Article **Journal Renewable Energy**
June, 2023 Vol.7 No.18 25-31

Economic and environmental dispatch of power systems: Minimising CO_2 emissions by integrating renewable energy sources

Despacho económico y medioambiental de los sistemas eléctricos: Minimización de las emisiones de CO_2 mediante la integración de fuentes de energía renovables

GARCÍA-GUZMÁN, José Miguel†*[1], RAZÓN-GONZÁLEZ, Juan Pablo[1], CANO-LARA, Miroslava[1] and GONZÁLEZ-PONCE, María del Refugio[2]

[1]*TecNM-Instituto Tecnológico Superior de Irapuato*
[2]*Universidad Incarnate Word Campus Bajío*

ID 1st Author: *José Miguel, García-Guzmán* / **ORC ID**: 0000-0003-4904-6213, **CVU CONAHCYT ID**: 470152

ID 1st Co-author: *Juan Pablo, Razón-González* / **ORC ID**: 0000-0002-9457-5029, **CVU CONAHCYT ID**: 216902

ID 2nd Co-author: *Miroslava, Cano-Lara* / **ORC ID**: 0000-0002-3335-2710, **CVU CONAHCYT ID**: 165249

ID 3rd Co-author: *María Del Refugio, González-Ponce* / **ORC ID**: 0000-0002-1170-2126, **CVU CONAHCYT ID**: 327208

DOI: 10.35429/JRE.2023.18.7.25.31 Received April 03, 2023; Accepted June 30, 2023

Abstract

This paper analyses the impact of the integration of renewable energy sources on the economic and environmental operation of power systems (PS). The models of renewable energy sources, as well as the generation cost function and Carbon Dioxide (CO_2) emissions are integrated in an Optimal Power Flow (OPF) formulation in order to obtain a non-linear multi-objective optimisation model, which considers economic and environmental aspects. This OPF model, having integrated the models of renewable energy sources, allows to evaluate the impact that these energy sources have on the minimisation of generation cost and CO_2 emissions. In this work, the multi-objective OPF problem is solved using weighting factors for the two functions considered in the global objective function. Several case studies are carried out to evaluate the effect of the integration of renewable energy sources on the economic and environmental operation of power systems. The results of the case studies show that renewable energy sources reduce generation cost and CO_2 emissions.

Renewable energy sources, Optimal generation dispatch, Power systems

Resumen

En este trabajo se analiza el impacto de la integración de las fuentes de energía renovable en la operación económica y ambiental de los sistemas eléctricos de potencia (SEP). Los modelos de las fuentes de energía renovable, así como la función de costo de generación y de emisiones de Dióxido de Carbono (CO_2) se integran en una formulación de Flujos de Potencia Óptimos (FPO) con la finalidad de obtener un modelo de optimización no lineal multi-objetivo, que considera aspectos económicos y ambientales. Este modelo de FPO, al tener integrados los modelos de las fuentes de energía renovable, permite evaluar el impacto que tienen estas fuentes de energía en la minimización del costo de generación y en las emisiones de CO_2. En este trabajo, el problema de FPO multi-objetivo se resuelve utilizando factores de ponderación para las dos funciones consideradas en la función objetivo global. Diversos casos de estudio se llevan a cabo para evaluar el efecto que tiene la integración de las fuentes de energía renovable en la operación económica y ambiental de los SEP. Los resultados de los casos de estudio muestran que las fuentes de energía renovable reducen el costo de generación y las emisiones de CO_2.

Fuentes de energía renovable, Despacho óptimo de generación, Sistemas eléctricos de potencia

Citation: GARCÍA-GUZMÁN, José Miguel, RAZÓN-GONZÁLEZ, Juan Pablo, CANO-LARA, Miroslava and GONZÁLEZ-PONCE, María del Refugio. Economic and environmental dispatch of power systems: Minimising CO_2 emissions by integrating renewable energy sources. Journal Renewable Energy. 2023. 7-18: 25-31

* Author Correspondence (e-mail: jose.gg@irapuato.tecnm.mx)
† Researcher contributing as first author.

Introduction

In recent years, care for the environment has become increasingly important in the daily and productive activities of society around the world. Therefore, it is of great importance nowadays to carry out such activities with minimal impact on the environment and to ensure environmental sustainability. Virtually all productive activities, especially those carried out at the industrial level, produce large amounts of pollutant gas emissions, known as greenhouse gases. Of all productive activities, in developed countries, electricity generation represents one of the main sources of environmental pollution through the emission of polluting gases into the atmosphere [Stott, 1979]. The greenhouse gases that power plants emit into the atmosphere in the greatest quantity are carbon monoxide, sulphur dioxide, nitrogen oxides and carbon dioxide, the latter being considered the greenhouse gas that contributes most to global warming, as it is the gas that is emitted in the greatest quantity by industry around the world [Atten et al, 2004; Demirel, 2004; Oceana, 2008; Rodríguez et al, 2013].

Mexico is one of the countries that, within the framework of the United Nations (UN) Paris Agreement [United Nations, 2015], have made specific commitments to curb global warming and climate change. The Nationally Determined Contributions (NDCs), together with the Special Climate Change Programme (SCCP), are Mexico's climate policy instruments, in which specific targets have been set to reduce 22% of its Greenhouse Gas (GHG) emissions, as well as to generate 35% of electricity through clean energy sources by 2024 and 43% by 2030, such generation to include renewable energy, cogeneration with natural gas and thermoelectric plants with CO_2 capture [CEMDA, s. f.; SEMARNAT, 2015].

For this reason, the integration of renewable energy sources into the active power generation system is of great importance, as it offers clean energy without greenhouse gas emissions, thus contributing to meeting the electrical energy demand of the power system with a decrease in GHG emissions, which reduces the carbon footprint that would occur if the demand were met solely by thermoelectric power plants.

As in the case of Mexico, policies, procedures and methods have been implemented around the world to minimise the effect of GHGs on air pollution. Policies and procedures include financial penalties for violation of permitted emission limits or green certificates to encourage the integration of clean energy sources in power systems. On the other hand, some of the common methods to reduce GHG gases are to reduce emissions from thermal power plants by using fuels with lower emission potential, installing post-combustion cleaning systems or dispatching generating units in such a way that emissions of polluting gases are minimised [Kulkarni et al, 2000; Song et al, 1997].

The analysis of Optimal Power Flows (OPF) allows the optimisation of an objective function subject to different equality and inequality constraints, thus determining the optimal steady-state operation of the power system. The objective functions can consider economic, safety or environmental aspects of the power system [Acha et al, 2004]. The objective function of the OPF problem can consider two aspects to be minimised simultaneously, obtaining a multi-objective OPF model, whose functions and constraints are non-linear.

In this work, the reduction of CO_2 emissions and the cost of active power generation are considered as objectives. It should be mentioned that the simultaneous reduction of CO_2 emissions and generation cost is a topic widely studied by utilities and researchers [Demirel, 2004; Dhillon et al, 1993; King, 1995; Kulkarni et al, 2000; Song et al, 1997]. However, the determination of the impact of renewable energies on the reduction of GHG emissions is not a common topic, since the mathematical modelling is complex and difficult to solve, due to the need to integrate the models of renewable energy sources in the formulation of multi-objective OPF, whose model is a highly non-linear optimisation problem with functional and variable constraints. This paper presents an analysis of the impact of the integration of renewable energy source models on the economic and environmental operation of power systems. The structure of the paper is as follows: The first section consists of the introduction and a review of the state of the art of the topic analysed in the paper, then in the next two sections the theoretical framework related to renewable energy sources and the multi-objective OPF problem is presented respectively.

ISSN 2523-2881

In the case studies section, several cases with a test power system are shown to evaluate the impact of renewable energy sources on the economic and environmental operation of the system. Finally, the penultimate and last section presents the conclusions obtained from the work and the bibliographical references, respectively.

Power generation from renewable energy sources

The renewable energy sources currently used to generate electricity are geothermal, ocean, bioenergy, hydro, solar and wind. Of these, wind and solar energy are the most prevalent in the world's electric power systems [Naciones Unidas, n. d.]. For this reason, these sources are the ones considered in this work.

A. Power generation by wind energy

In general, wind energy is produced by wind turbines or windmills. The kinetic energy in the moving air causes the turbine blades to rotate, whereby the kinetic energy is converted into mechanical energy, which in turn is converted into electrical energy by an electric generator, whose operation is based on an induction motor with negative torque, also known as an induction generator [Chapman, 2012]. The turbine-generator set is known as a wind turbine. The available power that is converted by the wind turbine is [Mahaboob et al, 2021],

$$P_W = 0.5\,\rho\,A\,v^3\,C_P \tag{1}$$

Where ρ is the wind density with a value of 1,221 kg/m^3, A is the swept area of the wind turbine blades in m^2 and v is the wind speed in m/s. The C_P term is the Betz constant or power coefficient, whose value is equal to 59.3% [Ackerman, 2005].

B. Power generation by solar energy

Solar energy is the most abundant energy on the planet, does not generate emissions that pollute the environment, requires less maintenance and has a long duration time. One of the important points for solar power generation is the sun's radiation, which is captured by a photovoltaic panel that is used to convert the sun's radiation into electrical energy.

A typical PV panel consists of a P-N junction semiconductor diode [Patel, 1999], which works on the principle of the photovoltaic effect, since when radiation strikes the diode, the P-N junction absorbs light and produces electric current. The power output generated by a P_S solar plant can be calculated, in kW, as follows [Mahaboob et al, 2005], only in case the solar irradiation is known.

$$P_S = PR\ GHI\ \eta_{PV}\ A_S\ S_Z \tag{2}$$

Where, the *PR* term is the performance ratio, whose value is dimensionless and lies between 0.5 and 0.9, the default value normally considered for this parameter is 0.75. The *GHI* term is the global horizontal irradiation in kW/m^2, A_S is the surface area of the solar panel in m^2, η_{PV} is the efficiency of the solar panel whose value is around 0.15 and S_Z is the number of solar panels contained in the solar plant.

Multi-objective OPF formulation considering renewable energy sources

The two objective functions to be minimised in the multi-objective OPF are the cost of active power generation and CO_2 emissions, both of which are minimised simultaneously. The mathematical formulation of this OPF problem considering the integration of solar and wind renewable energy sources is described below.

A. Mathematical model of the multi-objective OPF problem

1) Objective Function

The cost of active power generation involves maintenance costs, fixed costs, labour, fuel, among others, and is given by the following objective function,

$$F_C = \sum_{i=1}^{N_g} \left(a_i + b_i P_{g,i} + c_i P_{g,i}^{\ 2} \right) \tag{3}$$

In the above expression, it is clear that the function is non-linear. The terms a_i, b_i and c_i are the coefficients of the cost curves of the generators and $P_{g,i}$ is the power generated by each power plant connected to node i.

Similarly, the total CO_2 emissions from the combustion of thermal power plants can be modelled by the quadratic function given by (4).

ISSN 2523-2881

$$F_E = \sum_{i=1}^{N_g} \left(d_i + e_i P_{g,i} + f_i P_{g,i}{}^2 \right) \quad (4)$$

In the above equation, the terms d_i, e_i and f_i are the coefficients of the curves representing carbon dioxide emissions to the atmosphere. The valve points are not considered in this work [Demirel, 2004; Dhillon et al, 1993; King, 1995; Kulkarni et al, 2000; Song et al, 1997]. In both objective functions N_g is the number of generators installed in the power system.As mentioned, the sum of the generation cost function F_C and the emissions function F_E gives rise to the global multi-objective function [Demirel, 2004; Kulkarni et al, 2000], which is the new function to minimise in the OPF problem and is given as follows,

$$F_T \left(P_{g,i} \right) = w_C F_C (P_{g,i}) - w_E h F_E (P_{g,i}) \quad (5)$$

The terms w_C and w_E are the weighting coefficients for the cost and emissions functions, respectively, while the term h is the penalty factor that allows combining both objective functions into an overall function.

$$h_i = \frac{F_{Ci} \left(P_{gi}^{\max} \right) / P_{gi}^{\max}}{F_{Ei} \left(P_{gi}^{\max} \right) / P_{gi}^{\max}} \quad (6)$$

Where $P_{gi}{}^{max}$ is the maximum power of generator i, so that the cost and emission functions, F_{Ci} and F_{Ei}, are evaluated at this value of the power generated at the *i-th* generator.

2) Equality Constraints

The equality constraints that allow modelling the active power balance at node k considering the renewable energy sources are given as follows,

$$P_{g,k} + \sum_{i=1}^{N} P_{RES,i} - P_{D,k} - \sum_{k=1}^{Nb} P_{iny,k} = 0 \quad (7)$$

$$Q_{g,k} - Q_{D,k} - \sum_{m=1}^{Nb} Q_{iny,k} = 0 \quad (8)$$

Where $\{P_{g,k}, Q_{g,k}\}$, $\{P_{D,k}, Q_{D,k}\}$ and $\{P_{iny,k}, Q_{iny,k}\}$ are the active and reactive power generated, demanded and injected at node k, respectively. The term P_{RES}=$\{P_S, P_W\}$ represents the active power generated by the N renewable energy sources connected at node i. P_S is the power generated by photovoltaic power plants and P_W is the power generated by wind power plants.

3) Inequality constraints

Inequality constraints allow modelling the physical and operational limits of the power system, these limits are usually applied to the variables and sometimes to the functions that depend on the variables that determine the operating state of the power system. These limits are modelled by means of the following inequality constraints.

$$\delta_k^{\min} < \delta_k < \delta_k^{\max} \quad (9)$$

$$V_k^{\min} < V_k < V_k^{\max} \quad (10)$$

$$P_{g,i}^{\min} < P_{g,i} < P_{g,i}^{\max} \quad (11)$$

$$Q_{g,i}^{\min} < Q_{g,i} < Q_{g,i}^{\max} \quad (12)$$

$$P_W = \begin{cases} 0 & \text{if} \quad v < v_{\min} \\ 0.5 \rho A v^3 & \text{if} \quad v_{\min} < v < v_{\max} \\ P_r & \text{if} \quad v > v_{\max} \end{cases} \quad (13)$$

$$P_S = \begin{cases} 0 & \text{if} \quad GHI < GHI_{\min} \\ PR\ A_S\ S_Z\ \eta & \text{if} \quad GHI > GHI_{\min} \end{cases} \quad (14)$$

It should be noted that all the above expressions are inequality constraints to variables, except constraint (12), which is an inequality constraint to function, since reactive power depends on voltage. On the other hand, inequality constraints (13) and (14) correspond to renewable energy sources [Mahaboob et al, 2021]. The variable P_r is the rated power of the wind turbine, v_{min} is the minimum wind speed of 3.5 m/s and v_{max} is the maximum wind speed of 20 m/s. It should be mentioned that the nominal wind speed given in the literature is 11 m/s. The variable GHI_{min} is the minimum irradiance from the sun whose average value is 5.5 kW/m^2 [Deloitte, 2019].

Study cases

In this section, several study cases are presented to analyse the effect of integrating renewable energy source models on CO_2 emissions and the cost of active power generation of a power system.

ISSN 2523-2881

The 9-node test power system [Sauer, 1997] is used in the study cases presented his coefficients of both the generation cost functions and carbon dioxide emissions of the generators used in the case studies of this power system are shown in Table 1.

Generation cost coefficients			
Gen	**a ($/hr)**	**b ($/MWhr)**	**c ($/MW²hr)**
1	140	2.0	0.0060
2	120	1.5	0.0075
3	80	1.8	0.0070
CO_2 emission coefficients			
Gen	**d (lb/hr)**	**e (lb/MWhr)**	**F (lb/MW²hr)**
1	137.3701	-1.2488	0.0138
2	137.3701	-1.2488	0.0138
3	363.7048	0.8051	0.0077

Tabla 1 Coefficients of the cost and emission functions of the 9-node power system

The voltage limits used in the study cases presented with this power system are 0.95 pu for the lower limits and 1.05 pu for the upper limits. While the limits used for active and reactive power for generator 1 are, respectively, $0 \leq P_{G1} \leq 200$ MW and $-100 \leq Q_{G1} \leq 150$ MVAR; for generator of $0 \leq P_{G2} \leq 150$ MW and $-100 \leq Q_{G2} \leq 300$ MVAR; and for generator 3 of $0 \leq P_{G3} \leq 100$ MW and $-100 \leq Q_{G3} \leq 300$ MVAR. The initial conditions of the voltage phase angles are 0°.

First, the multi-objective OPF is solved to determine the economic and environmental dispatch of the 9-node power system without considering the integration of the renewable energy source models. This case is considered as the base case. Subsequently, two study cases are carried out in which the renewable energy source models are integrated in a) the energy supply nodes and b) in the nodes where the greatest amount of load is installed, in order to observe the effect that clean energies have in the different SEP operating areas.

In both cases, a wind power plant with a generation capacity of 35,725 MW and a photovoltaic power plant with an active power of 48,094 MW are integrated simultaneously. It is important to mention that in the OPF analyses carried out, the cost function and the emissions function are combined in the global function with the same weight factor, in order to analyse the operation of the power system, giving equal importance to the economic and environmental aspects.

In the first case study, a wind power plant is integrated at node 7 and a photovoltaic power plant at node 9, both of which are nodes at which energy is supplied to the power system. A brief comparison of results with and without the integration of renewable energy sources is presented in Table 2, while Figure 1 shows the voltage profile obtained when renewable energy sources are integrated.

Parameters	Without P_W y P_S	With P_W y P_S
P_G (MW)	318.001	235.36
Q_G (MVAR)	5.818	2.44
P_{losses} (MW)	3.001	4.177
Q_{losses} (MVAR)	-109.182	-112.551
Cost ($/hr)	1134.055	885.492
Emissions (lb/hr)	845.603	702.8172
Global objective function	1129.8	910.526

Tabla 2 Summary of results with and without simultaneously connected renewable energy sources at the energy supply nodes

In the second case, wind and PV power plants are integrated at load nodes 5 and 6, respectively. A summary of the results for this case study is shown in Table 3, which compares these results with those obtained in the base case.

Parameters	Without P_W y P_S	With P_W y P_S
P_G (MW)	318.001	232.49
Q_G (MVAR)	5.818	-12.64
P_{losses} (MW)	3.001	1.307
Q_{losses} (MVAR)	-109.182	-127.646
Cost ($/hr)	1134.055	878.183
Emissions (lb/hr)	845.603	699.995
Global objective function	1129.8	904.992

Tabla 3 Summary of results with and without simultaneously connected renewable energy sources at load nodes

As expected, the results presented in the tables above show that integrating renewable energy sources decreases active power generation because less power is demanded from the generators to meet the load and losses in the transmission elements. It is clear that reducing active power generation reduces both the cost of generation and carbon dioxide emissions. It is important to emphasise that, according to the results shown, generation costs and CO_2 emissions decrease when renewable generation plants are installed close to consumption centres, due to the decrease in transmission element losses.

ISSN 2523-2881

However, it is sometimes not possible to install clean power plants close to loads, as they are limited to the availability of wind and sun. Fortunately, in Mexico there is photovoltaic potential over the entire surface of the country, which can favour a location of renewable energy plants as close as possible to load centres, in order to improve the economic and environmental operation of power systems. On the other hand, with the integration of renewable energy sources, generation and reactive power losses are reduced, which translates into an improvement in the nodal voltage profile of the power system, as shown in Graphic 1. Node 5 has a lower voltage, as it is the node where the largest load is connected to the power system. The integration of wind and photovoltaic power plants at the energy supply nodes of the power system does not cause significant changes, unlike the case in which they are installed at the load nodes.

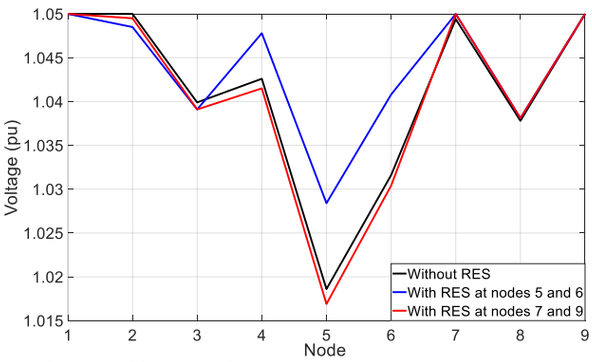

* RES: Renewable Energy Sources.

Graphic 1 Nodal voltage profile considering the effect of renewable energy sources

Finally, it should be noted that active power losses are higher when adding renewable energy sources to the power system, which is due to the redistribution of power flows that occur in the system.

Conclusions

An analysis of the economic and environmental dispatch, where CO2 emissions and the cost of active power generation are minimised by integrating the wind and solar energy source models, has been presented. According to the results obtained, it can be concluded that by integrating the renewable energy source models there is a reduction in carbon dioxide emissions and generation cost, thus improving the economic and environmental operation of the power system, despite the increase in active power losses.

Similarly, it is concluded that the integration of renewable energy sources improves the nodal voltage profile of the system due to a decrease in generation and reactive power losses. Finally, it should be mentioned that the cost of generation and carbon dioxide emissions decrease considerably when generation plants with renewable energy sources are installed close to power consumption centres.

This work has been funded by ITESI and CONAHCYT under de research project CI-01-2022.

References

Acha E., Fuerte C. R., Ambriz H. and Ángeles C. C. (2004). *FACTS: Modelling and Simulation in Power Networks*. John Wiley & Sons. DOI:10.1002/0470020164

Ackerman T. (2005). *Wind Power in Power Systems*. John Wiley & Sons. DOI:10.1002/0470012684.ch7

Atten C. V., Bradley M. J. y Miller P. J. (2004). *Emisiones atmosféricas de las centrales eléctricas en América del Norte. Comisión para la Cooperación Ambiental de América del Norte*
http://www3.cec.org/islandora/es/item/2165-north-american-power-plant-air-emissions-es.pdf.

CEMDA. (s. f.). *Avance del cumplimiento de los compromisos internacionales de México para combatir el cambio climático*. Consultado el 19 de Mayo de 2023. https://www.cemda.org.mx/avance-del-cumplimiento-de-los-compromisos-internacionales-de-mexico-para-combatir-el-cambio-climatico/#:~:text=ACCIONES%20DEFINIDAS%20POR%20M%C3%89XICO%20EN,en%20equipos%20e%20instalaciones%20industriales

Chapman, S. J. (2012). *Máquinas Eléctricas.* McGraw-Hill Interamericana de España S. L.

Deloitte México. (2019). *En energía, México debe apuntar al sol*. https://www2.deloitte.com/mx/es/pages/dnoticias/articles/energia-solar-en-mexico.html.

ISSN 2523-2881

Demirel Y. and Demiroren A. (2004). Economic and minimum emission dispatch. *Transactions on Systems*, 3(2), 364-368. https://www.researchgate.net/publication/237469701_ECONOMIC_AND_MINIMUM_EMISSION_DISPATCH

Dhillon J. S., Parti S. C. and Kothari D. P. (1993). Stochastic Economic Emission Load Dispatch. *Electric Power Systems Research*, 26(3), 179-186. DOI: 10.1016/0378-7796(93)90011-3.

King T. D., El-Hawary M. E. and El-Hawary F. (1995). Optimal environmental dispatching of electric power systems via an improved Hopfield neural network model. *IEEE Transactions on Power Systems*, 10(3),1559-1565. DOI: 10.1109/59.466488.

Kulkarni P. S., Kothari A. G. and Kothari D.P. (2000). Combined Economic and Emission Dispatch Using Improved Back Propagation Neural Network. *Electric Machines and Power Systems*, 28(1), 31-44. DOI: 10.1080/073135600268496

Mahaboob S. S., Chintalapudi S. V. and Sirigiri S. (2021). Optimal Power Flow Solution in the Presence of Renewable Energy Sources. *Iran J Sci Technol Trans Electr Eng*. 1(45), 61-79. https://doi.org/10.1007/s40998-020-00339-z

Naciones Unidas. (2015). *Acuerdo de París de la Convención Marco de las Naciones Unidas sobre el Cambio Climático (UNFCCC)*. https://www.refworld.org.es/docid/602021b64.

Naciones Unidas. (s. f.). *Acción por el clima - ¿Qué son las energías renovables?* Consultado el 19 de Mayo de 2023. https://www.un.org/es/climatechange/what-is-renewable-energy

Oceana. (2008). *Gases de efecto invernadero*. https://eu.oceada.org/es/

Patel. M. R. (1999). *Wind and solar power systems: design, analysis, and operation*. CRC Press. DOI:10.1201/9781003042952

Rodríguez L. F., Pérez S. M y Mora J. J. (2013). Estimación de parámetros de un modelo de carga de recuperación exponencial empleando técnicas metaheurísticas. *Scientia Et Technica*, 18(3), 453-462. https://www.redalyc.org/articulo.oa?id=84929154004

Sauer P. W. and Pai M. A. (1997). *Power System Dynamics and Stability*. Stipes Publishing L.L.C. https://courses.physics.illinois.edu/ece576/sp2018/Sauer%20and%20Pai%20book%20-%20Jan%202007.pdf

SEMARNAT. (2015). *Compromisos de mitigación y adaptación 2020-2030.* https://www.gob.mx/semarnat/articulos/compromisos-de-mitigacion-y-adaptacion-2020-2030

Song Y. H., Wang G.S., Wang P. Y. and Johns A. T. (1997). *Environmental / Economic Dispatch Using Fuzzy Logic Controlled Genetic Algorithms*. IEEE Proceedings, Generation, Transmission and Distribution, 144(4), 377-382. DOI: 10.1049/ip-gtd:19971100.

Stott B. (1979 Febrero). *Power system dynamic response calculations*. Proceedings of the IEEE. DOI: 10.1109/PROC.1979.11233.

ISSN 2523-2881

[Title in Times New Roman and Bold No. 14 in English and Spanish]

Surname (IN UPPERCASE), Name 1st Author†*, Surname (IN UPPERCASE), Name 1st Coauthor, Surname (IN UPPERCASE), Name 2nd Coauthor and Surname (IN UPPERCASE), Name 3rd Coauthor

Institutional Affiliation of Author including Dependency (No.10 Times New Roman and Italic)

International Identification of Science - Technology and Innovation

ID 1st Author: (ORC ID - Researcher ID Thomson, arXiv Author ID - PubMed Author ID - Open ID) and CVU 1st author: (Scholar-PNPC or SNI-CONAHCYT) (No.10 Times New Roman)

ID 1st Coauthor: (ORC ID - Researcher ID Thomson, arXiv Author ID - PubMed Author ID - Open ID) and CVU 1st coauthor: (Scholar or SNI) (No.10 Times New Roman)

ID 2nd Coauthor: (ORC ID - Researcher ID Thomson, arXiv Author ID - PubMed Author ID - Open ID) and CVU 2nd coauthor: (Scholar or SNI) (No.10 Times New Roman)

ID 3rd Coauthor: (ORC ID - Researcher ID Thomson, arXiv Author ID - PubMed Author ID - Open ID) and CVU 3rd coauthor: (Scholar or SNI) (No.10 Times New Roman)

(Report Submission Date: Month, Day, and Year); Accepted (Insert date of Acceptance: Use Only ECORFAN)

Abstract (In English, 150-200 words)

Objectives
Methodology
Contribution

Abstract (In Spanish, 150-200 words)

Objectives
Methodology
Contribution

Keywords (In English)

Indicate 3 keywords in Times New Roman and Bold No. 10

Keywords (In Spanish)

Indicate 3 keywords in Times New Roman and Bold No. 10

Citation: Surname (IN UPPERCASE), Name 1st Author, Surname (IN UPPERCASE), Name 1st Coauthor, Surname (IN UPPERCASE), Name 2nd Coauthor and Surname (IN UPPERCASE), Name 3rd Coauthor. Paper Title. Journal Renewable Energy. Year 1-1: 1-11 [Times New Roman No.10]

* Correspondence to Author (example@example.org)
† Researcher contributing as first author.

Introduction

Text in Times New Roman No.12, single space.

General explanation of the subject and explain why it is important.

What is your added value with respect to other techniques?

Clearly focus each of its features

Clearly explain the problem to be solved and the central hypothesis.

Explanation of sections Article.

Development of headings and subheadings of the article with subsequent numbers

[Title No.12 in Times New Roman, single spaced and bold]

Products in development No.12 Times New Roman, single spaced.

Including graphs, figures and tables-Editable

In the article content any graphic, table and figure should be editable formats that can change size, type and number of letter, for the purposes of edition, these must be high quality, not pixelated and should be noticeable even reducing image scale.

[Indicating the title at the bottom with No.10 and Times New Roman Bold]

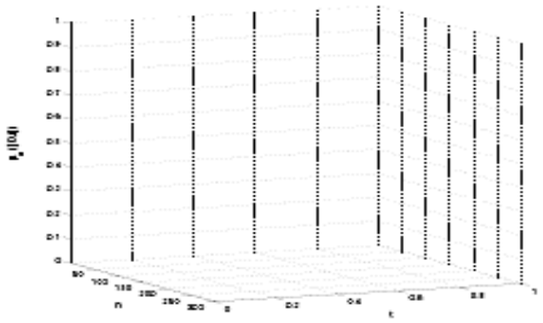

Graphic 1 Title and *Source (in italics)*

Should not be images-everything must be editable.

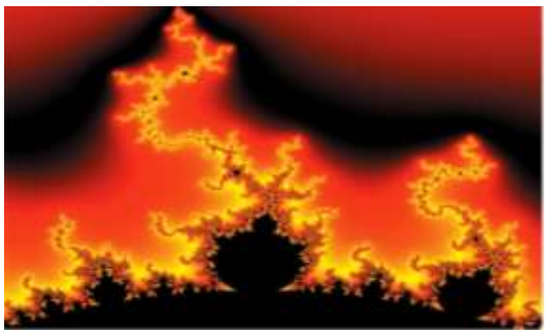

Figure 1 Title and *Source (in italics)*

Should not be images-everything must be editable.

Table 1 Title and *Source (in italics)*

Should not be images-everything must be editable.

Each article shall present separately in **3 folders**: a) Figures, b) Charts and c) Tables in .JPG format, indicating the number and sequential Bold Title.

For the use of equations, noted as follows:

$$Y_{ij} = \alpha + \sum_{h=1}^{r} \beta_h X_{hij} + u_j + e_{ij} \qquad (1)$$

Must be editable and number aligned on the right side.

Methodology

Develop give the meaning of the variables in linear writing and important is the comparison of the used criteria.

Results

The results shall be by section of the article.

Annexes

Tables and adequate sources

Thanks

Indicate if they were financed by any institution, University or company.

ISSN: 2523-2881

Conclusions

Explain clearly the results and possibilities of improvement.

References

Use APA system. Should not be numbered, nor with bullets, however if necessary numbering will be because reference or mention is made somewhere in the Article.

Use Roman Alphabet, all references you have used must be in the Roman Alphabet, even if you have quoted an Article, book in any of the official languages of the United Nations (English, French, German, Chinese, Russian, Portuguese, Italian, Spanish, Arabic), you must write the reference in Roman script and not in any of the official languages.

Technical Specifications

Each article must submit your dates into a Word document (.docx):

Journal Name
Article title
Abstract
Keywords
Article sections, for example:

1. Introduction
2. Description of the method
3. Analysis from the regression demand curve
4. Results
5. Thanks
6. Conclusions
7. References

Author Name (s)
Email Correspondence to Author
References

Intellectual Property Requirements for editing:

- Authentic Signature in Color of Originality Format Author and Coauthors
- Authentic Signature in Color of the Acceptance Format of Author and Coauthors
- Authentic Signature in Color of the Conflict of Interest Format of Author and Co-authors.

ISSN: 2523-2881

Reservation to Editorial Policy

Journal Renewable Energy reserves the right to make editorial changes required to adapt the Articles to the Editorial Policy of the Research Journal. Once the Article is accepted in its final version, the Research Journal will send the author the proofs for review. ECORFAN® will only accept the correction of errata and errors or omissions arising from the editing process of the Research Journal, reserving in full the copyrights and content dissemination. No deletions, substitutions or additions that alter the formation of the Article will be accepted.

Code of Ethics - Good Practices and Declaration of Solution to Editorial Conflicts

Declaration of Originality and unpublished character of the Article, of Authors, on the obtaining of data and interpretation of results, Acknowledgments, Conflict of interests, Assignment of rights and Distribution.

The ECORFAN-Mexico, S.C Management claims to Authors of Articles that its content must be original, unpublished and of Scientific, Technological and Innovation content to be submitted for evaluation.

The Authors signing the Article must be the same that have contributed to its conception, realization and development, as well as obtaining the data, interpreting the results, drafting and reviewing it. The Corresponding Author of the proposed Article will request the form that follows.

Article title:

- The sending of an Article to Journal Renewable Energy emanates the commitment of the author not to submit it simultaneously to the consideration of other series publications for it must complement the Format of Originality for its Article, unless it is rejected by the Arbitration Committee, it may be withdrawn.

- None of the data presented in this article has been plagiarized or invented. The original data are clearly distinguished from those already published. And it is known of the test in PLAGSCAN if a level of plagiarism is detected Positive will not proceed to arbitrate.

- References are cited on which the information contained in the Article is based, as well as theories and data from other previously published Articles.

- The authors sign the Format of Authorization for their Article to be disseminated by means that ECORFAN-Mexico, S.C. In its Holding Republic of Peru considers pertinent for disclosure and diffusion of its Article its Rights of Work.

- Consent has been obtained from those who have contributed unpublished data obtained through verbal or written communication, and such communication and Authorship are adequately identified.

- The Author and Co-Authors who sign this work have participated in its planning, design and execution, as well as in the interpretation of the results. They also critically reviewed the paper, approved its final version and agreed with its publication.

- No signature responsible for the work has been omitted and the criteria of Scientific Authorization are satisfied.

- The results of this Article have been interpreted objectively. Any results contrary to the point of view of those who sign are exposed and discussed in the Article.

Copyright and Access

The publication of this Article supposes the transfer of the copyright to ECORFAN-Mexico, SC in its Holding Republic of Peru for its Journal Renewable Energy, which reserves the right to distribute on the Web the published version of the Article and the making available of the Article in This format supposes for its Authors the fulfilment of what is established in the Law of Science and Technology of the United Mexican States, regarding the obligation to allow access to the results of Scientific Research.

Article Title:

Name and Surnames of the Contact Author and the Coauthors	Signature
1.	
2.	
3.	
4.	

Principles of Ethics and Declaration of Solution to Editorial Conflicts

Editor Responsibilities

The Publisher undertakes to guarantee the confidentiality of the evaluation process, it may not disclose to the Arbitrators the identity of the Authors, nor may it reveal the identity of the Arbitrators at any time.

The Editor assumes the responsibility to properly inform the Author of the stage of the editorial process in which the text is sent, as well as the resolutions of Double-Blind Review.

The Editor should evaluate manuscripts and their intellectual content without distinction of race, gender, sexual orientation, religious beliefs, ethnicity, nationality, or the political philosophy of the Authors.

The Editor and his editing team of ECORFAN® Holdings will not disclose any information about Articles submitted to anyone other than the corresponding Author.

The Editor should make fair and impartial decisions and ensure a fair Double-Blind Review.

Responsibilities of the Editorial Board

The description of the peer review processes is made known by the Editorial Board in order that the Authors know what the evaluation criteria are and will always be willing to justify any controversy in the evaluation process. In case of Plagiarism Detection to the Article the Committee notifies the Authors for Violation to the Right of Scientific, Technological and Innovation Authorization.

Responsibilities of the Arbitration Committee

The Arbitrators undertake to notify about any unethical conduct by the Authors and to indicate all the information that may be reason to reject the publication of the Articles. In addition, they must undertake to keep confidential information related to the Articles they evaluate.

Any manuscript received for your arbitration must be treated as confidential, should not be displayed or discussed with other experts, except with the permission of the Editor.

The Arbitrators must be conducted objectively, any personal criticism of the Author is inappropriate.

The Arbitrators must express their points of view with clarity and with valid arguments that contribute to the Scientific, Technological and Innovation of the Author.

The Arbitrators should not evaluate manuscripts in which they have conflicts of interest and have been notified to the Editor before submitting the Article for Double-Blind Review.

Responsibilities of the Authors

Authors must guarantee that their articles are the product of their original work and that the data has been obtained ethically.

Authors must ensure that they have not been previously published or that they are not considered in another serial publication.

Authors must strictly follow the rules for the publication of Defined Articles by the Editorial Board.

The authors have requested that the text in all its forms be an unethical editorial behavior and is unacceptable, consequently, any manuscript that incurs in plagiarism is eliminated and not considered for publication.

Authors should cite publications that have been influential in the nature of the Article submitted to arbitration.

Information services

Indexation - Bases and Repositories

LATINDEX (Scientific Journals of Latin America, Spain and Portugal)
EBSCO (Research Database - EBSCO Industries)
RESEARCH GATE (Germany)
GOOGLE SCHOLAR (Citation indices-Google)
MENDELEY (Bibliographic References Manager)
HISPANA (Information and Bibliographic Orientation-Spain)

Publishing Services

Citation and Index Identification H
Management of Originality Format and Authorization
Testing Article with PLAGSCAN
Article Evaluation
Certificate of Double-Blind Review
Article Edition
Web layout
Indexing and Repository
ArticleTranslation
Article Publication
Certificate of Article
Service Billing

Editorial Policy and Management

1047 La Raza Avenue -Santa Ana, Cusco-Peru. Phones: +52 1 55 6159 2296, +52 1 55 1260 0355, +52 1 55 6034 9181; Email: contact@ecorfan.org www.ecorfan.org

Journal Renewable Energy

"Design of a p-i-n type inverted perovskite solar cell using SiO_x as down-conversion material to improve PCE: Simulation and optimization in SCAPS-1D"
PAZ-TOTOLHUA, Ezequiel, CARRILLO-LÓPEZ, Jesús, LUNA-LÓPEZ, José Alberto and BENÍTEZ-LARA, Alfredo
Benemérita Universidad Autónoma de Puebla

"Low-cost Schlieren system for flow visualization in transparent media in the wind sector"
URIBE-CASTILLO, Citlali & RICO-ESPINO, José Guadalupe
Universidad Tecnológica de Querétaro

"Effect of dye on the efficiency of Grätzel cells"
BERNAL-MARTINEZ, Guillermo, MONTES-GUTIERREZ, Jorge, GARCIA-GUTIERREZ, Rafael and CONTRERAS-LOPEZ, Oscar
Centro de Investigación Científica y de Educación Superior de Ensenada
Universidad Nacional Autónoma de México
Universidad de Sonora

"Economic and environmental dispatch of power systems: Minimising CO_2 emissions by integrating renewable energy sources"
GARCÍA-GUZMÁN, José Miguel, RAZÓN-GONZÁLEZ, Juan Pablo, CANO-LARA, Miroslava and GONZÁLEZ-PONCE, María del Refugio
Instituto Tecnológico Superior de Irapuato
Universidad Incarnate Word Campus Bajío

2523 6881
ISSN 2523 - 6881
www.ecorfan.org